The Moroccan High Atlas phosphate-rich sediments: Unraveling the accumulation and differentiation processes

Radouan El Bamiki, Michel Séranne, El Hassane Chellaï, Gilles Merzeraud, Mohamed Marzoqi, Mihaela Carmen Melinte-Dobrinescu

To cite this version:

Radouan El Bamiki, Michel Séranne, El Hassane Chellaï, Gilles Merzeraud, Mohamed Marzoqi, et al.. The Moroccan High Atlas phosphate-rich sediments: Unraveling the accumulation and differentiation processes. Sedimentary Geology, 2020, 403, pp.105655. 10.1016/j.sedgeo.2020.105655 . hal-02871048

HAL Id: hal-02871048
https://hal.umontpellier.fr/hal-02871048

Submitted on 24 Nov 2020

HAL is a multi-disciplinary open access archive for the deposit and dissemination of scientific research documents, whether they are published or not. The documents may come from teaching and research institutions in France or abroad, or from public or private research centers.

L'archive ouverte pluridisciplinaire HAL, est destinée au dépôt et à la diffusion de documents scientifiques de niveau recherche, publiés ou non, émanant des établissements d'enseignement et de recherche français ou étrangers, des laboratoires publics ou privés.

The Moroccan High Atlas phosphate-rich sediments:

unraveling the accumulation and differentiation processes

Radouan El Bamiki[1,2*], Michel Séranne[2], El Hassane Chellaï[1], Gilles Merzeraud[2], Mohamed Marzoqi[1], Mihaela Carmen Melinte-Dobrinescu[3]

(1) Department of Geology, Faculty of Sciences Semlalia, Cadi Ayyad University, Prince Moulay Abdellah Av. Marrakesh 40000, Morocco.

(2) UMR CNRS 5243 Geosciences Montpellier, University of Montpellier, CC 060, Pl. Eugène Bataillon, 34095 Montpellier Cedex 05, France.

(3) National Institute of Marine Geology and Geoecology, 23-25 Dimitrie Onciul street, P.O. Box 34-51, 70318 Bucharest, Romania.

12   **Abstract**

13   The phosphate series of the Moroccan High Atlas accumulated during the Upper

14   Cretaceous-Paleogene phosphogenic period, on a biologically-productive shallow-water

15   platform. These phosphate-rich sediments were deposited during a relative sea-level

16   cycle generating major stratigraphic surfaces. Five different types of phosphate

17   lithofacies are recognized, based on their petrographic and sedimentologic features. The

18   *pristine phosphate* lithofacies corresponds to phosphatic marls formed by francolite

19   authigenesis within the outer platform domain below the storm wave-base (primary

20   phosphogenesis zone). This primary phosphate lithofacies can be differentiated as a

21   result of the interaction between hydrodynamic autocyclic processes and allocyclic

22   forcing. Accordingly, the *granular phosphate* lithofacies was formed by in-situ storm and

23   bottom currents that winnowed the pristine phosphate. This winnowed lithofacies,

24   composed of densely-packed peloids, shows relatively high P_2O_5 concentrations. The

25   *turbiditic phosphate* resulted from the basinward transport and deposition of other

26   phosphate types by gravity flows leading to normally-graded phosphate sediment. The

27   *phosphatic lags* were formed by wave reworking and transporting of pristine and

28   associated granular facies within the inner platform. The *karst-filling phosphate*

29   corresponds to former phosphate types transported by early transgressive currents and

30   trapped within karstic pockets as microconglomeratic phosphate. The distribution of the

31   different phosphate types across the margin and within the depositional sequences is

32   controlled by the effects of relative sea-level changes. The pristine phosphate and

33   associated winnowed facies are found above the major maximum flooding surface, which

34   is dated by nannoflora to the Selandian-Thanetian transition. The phosphatic turbidites

35   occurred during periods of high sea-level. The karst-related phosphatic facies

2

accumulated during early transgressive stages. The phosphatic lags accumulated mainly during the regressive phases of third and fourth order sequences. The accumulation processes of the different phosphate lithofacies control the ore grade of the phosphatic sediments: repeated storm-induced winnowing of pristine phosphate contributes to enrichment of the phosphate ore grade.

Keywords

1. Introduction

Sedimentary phosphate is a strategic phosphorus (P) resource, essential for agriculture and industry (Glenn et al., 1994). The processes controlling phosphogenesis (the authigenic precipitation of P-bearing minerals, mainly francolite which is a carbonate fluorapatite; Föllmi et al., 1993; Jarvis et al., 1994) have stimulated considerable discussion, giving rise to multiple theories (e.g., inorganic vs. organic precipitation of apatite; Trappe, 1998, and references therein). Major advances in phosphate geochemistry have led to a consensus on phosphogenesis involving biochemical processes (Glenn et al., 1994; Jarvis et al., 1994; Krajewski et al., 1994). Consequently, it has been demonstrated that phosphogenesis can occur in a large array of sedimentary environments, from deep basin areas to anoxic marginal basins (Filippelli, 2011). The diversity of sedimentary environments where phosphogenesis has been documented argues for diverse geochemical, hydrodynamic, and paleoenvironmental controls. Thus, phosphogenesis is not a unique process and it cannot lead by itself to phosphate-rich

58   sediments, without the intervention of post-phosphogenesis agents which facilitate ore

59   accumulation, concentration, and enrichment (Baturin, 1982). Despite their critical role

60   in the phosphate accumulation, these post-phosphogenesis agents remained

61   understudied. Phosphate-rich sediments are traditionally subdivided into primary and

62   reworked facies (e.g., Trappe, 1998, Follmi 1996, 2016; Glenn et al., 1994; Pufahl et al.,

63   2003; Soudry et al., 2013; Pufahl and Groat 2017). Primary or pristine phosphate refers

64   to phosphatic fine sediments preserved in their initial state without undergoing

65   transport or reworking. It is generally of low P_2O_5 content within the host sediment.

66   Reworked phosphate is regarded as typically granular facies deposited by hydrodynamic

67   reworking agents. It is of economic interest due to the concentration of phosphatic grains.

68   When concentration reaches 18%wt P_2O_5, it is named phosphorite (Slansky, 1986).

69   Phosphate accumulations occur preferentially on continental shelves and epeiric seas,

70   where the water depth allows permanent, periodic or occasional reworking of the water-

71   sediment interface (Baturin, 1982; Glenn et al., 1994; Föllmi, 1996; Pufahl and Groat,

72   2017).

73   The Upper Creataceous-Eocene interval is among the significant phosphogenic periods

74   known in the geological record (Pufahl and Groat, 2017). During this period, the Tethyan

75   province saw the formation of large sedimentary phosphate deposits which are now

76   exploited (Notholt 1985); e.g., in Algeria (Kechiched et al., 2018), Tunisia (Ounis et al.,

77   2008), and Egypt (Baioumy et al., 2007). Contemporaneous phosphate deposits of

78   Morocco correspond to the largest sedimentary phosphate reserve (70% of world-known

79   reserves; Jasinski, 2018). These deposits are currently mined in the central part of

80   Morocco (Meseta domain) and in the south, yet other occurrences exist along the High
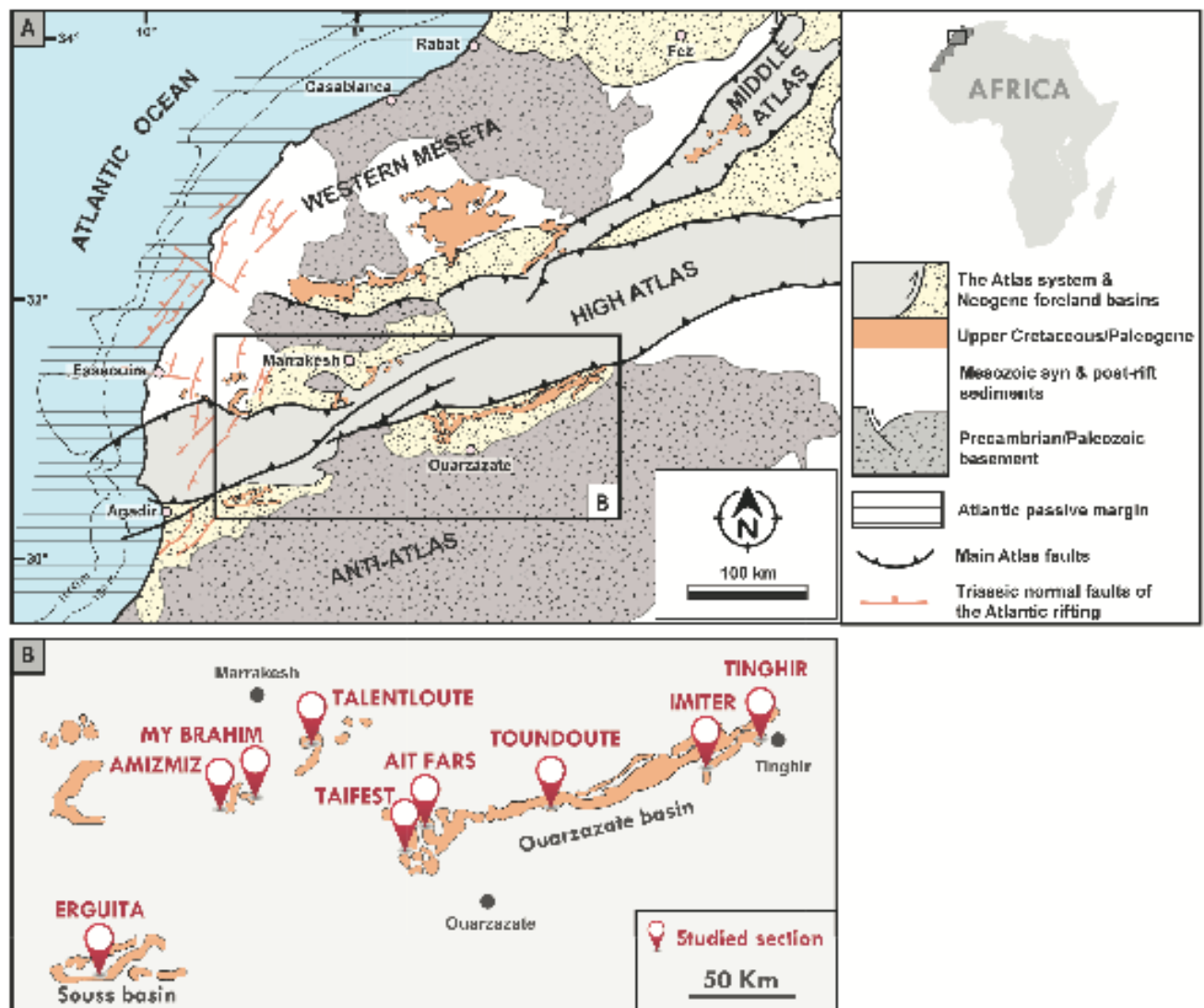
81   Atlas (Fig. 1A).

Fig. 1. (A) Simplified structural map of Morocco illustrating the spatial distribution of the Upper Cretaceous-Paleogene phosphate-rich sediments and highlighting the main structural and geodynamic features of the Moroccan Atlas system. Modified after Hafid et al. (2006). (B) Location of the investigated sections along the northern and southern borders of the High Atlas system.

The exploited phosphate deposits of the Meseta have been extensively and repeatedly studied since first discoveries of phosphate in Morocco by Brives (1905). Previous work focused on phosphate petrography and granulometry (Salvan, 1986; Mouflih, 2015), and geochemistry (Belfkira, 1980; Prévôt, 1988). Basin-scale studies were conducted for

mining purposes (Boujo, 1976; Belfkira, 1980; Salvan, 1986; Gharbi, 1998). The phosphate series of Morocco has attracted paleontologists for its extraordinary and well-preserved vertebrate fauna (see Bardet et al., 2017, for review).

In spite of these numerous studies on the Moroccan phosphate series, accumulation and preservation processes are poorly known. The relationship between sedimentary processes and phosphate accumulation is still not well constrained. The exploited phosphorites correspond to extensive, thin, tabular beds accumulated by reworking (Belfkira, 1980; Boujo, 1976). However, there is this far, no record of the original pristine phosphate sediments. Consequently, the succession of events between primary phosphogenesis and final phosphorite accumulation and preservation remains unknown.

The presently exploited phosphorites basins of the Moroccan Meseta are flat-lying, often covered by Pliocene to Recent sediment. Sections are only visible along the active excavations of the open-cast mines, which are difficult to access for scientific investigations. For these reasons, we targeted the contemporaneous phosphate-bearing series along the High Atlas margins offering excellent section exposures of the folded Cretaceous to Eocene sequences, which allows stratigraphic correlation. The purpose of this study is to unravel the different processes behind the concentration and accumulation of phosphate-rich sediments of the Moroccan High Atlas, using sedimentologic and sequence stratigraphic tools. We present a detailed facies and facies association analysis, describe and interpret the different accumulation modes of phosphate, and establish the sequence stratigraphic framework of the studied series. This requires a well-defined stratigraphic framework. In this study, we trace the post-genesis pathways of phosphatic grains and the interaction between sea-level variations and phosphate deposition. We analyze the lateral evolution of phosphate types across the

125 basin, and propose an integrated model for the phosphate accumulation within the High

126 Atlas of Morocco.

2. Geological setting

128 The investigated Upper Cretaceous-Paleogene sedimentary successions are located along

129 the northern and southern borders of the NE-striking High Atlas belt of Morocco, in the

130 Marrakech - Ouarzazate area (Fig. 1A). This orogen corresponds to a Mesozoic-Paleogene

131 intracontinental basin (Atlasic Basin), which was inverted during the Neogene (Michard

132 et al., 2008; Frizon de Lamotte et al., 2009). The mountain range exhibits double verging

133 thrusts, resulting in high tabular plateaus in the axial part (Fekkak et al., 2018).

134 The evolution of the High Atlas started in the Triassic with the creation of the Atlasic

135 basins linked to the Central Atlantic rifting and the formation of the Atlantic passive

136 margin (Tucholke et al., 2007; Schettino and Turco, 2009; Frizon De Lamotte et al., 2015).

137 The basins have recorded important post-rift, thermally-enhanced subsidence of the

138 Atlantic margin (Ellouz et al., 2003), leading to the deposition of thick sequences of

139 Mesozoic sediments. The thermal cooling faded away with time and by the Upper

140 Cretaceous period, subsidence had drastically decreased (Ellouz et al., 2003; Tari et al.,

141 2012). Consequently, relatively thin Paleogene successions, including the phosphate

142 series, accumulated in the Atlasic basin.

143 The major uplift and inversion event of the High Atlas was initiated during the Neogene,

144 i.e., postdating deposition of phosphate-rich sequences. The former syn-rift faults were

145 reactivated and inverted in response to the convergence between Africa and Eurasia

146 plates (e.g., Beauchamp et al., 1999; Frizon de Lamotte et al., 2009; Frizon De Lamotte et

7

al., 2015). This ongoing uplift is also enhanced by deep thermal processes (Leprêtre et al., 2015; Missenard et al., 2008; Teixell et al., 2005). Foreland basins were created north (Marrakesh), and south (Ouarzazate and Souss) of the orogen and filled with continental molassic sediments delivered by the erosion of the uprising belt (Görler et al., 1988; Chellai and Perriaux, 1996; El Harfi et al., 2001; Michard et al., 2008).

The phosphate-rich sediments of the Moroccan High Atlas belong to the late Cretaceous-Paleogene stratigraphic interval (Trappe, 1991; Chellaï et al., 1995; Marzoqi and Pascal, 2000). At that time, the Atlas phosphate basins were bordered to the south by the large Paleozoic fold belt of the Anti-Atlas, constituting the southern hinterland area, and to the north and east by the deformed Variscan basement of the Western Meseta (Herbig and Trappe, 1994). These phosphate basins extended westwards to the Atlantic passive margin and the westward thickening of the formations (Boujo, 1976) is related to the increasing subsidence towards the passive margin. These phosphate accumulations are hosted by a marine-dominated sedimentary succession displaying shallow-water platform environments (Fig. 2). They are bounded by under- and overlying continental sediments. The phosphate series of the High Atlas is subdivided into two sedimentary systems separated by a regional-scale discontinuity formed during a second-order transgressive-regressive cycle (Chellaï et al., 1995; Marzoqi and Pascal, 2000).

3. Methodology

This work is based on nine sections, measured along the margins of the Moroccan High Atlas (Fig. 1B). They extend over 300 km from northeast to southwest and over 100 km from the southeast, close to the Anti-Atlas Precambrian basement, to the northwest in the Marrakesh area. Detailed field measurements were carried out, based on bed-by-bed

description. We sampled the studied series in multiple locations for petrographic and

biostratigraphic purposes. We defined facies and facies associations based on field and

petrographic observations, which allowed to interpret the sedimentary processes and
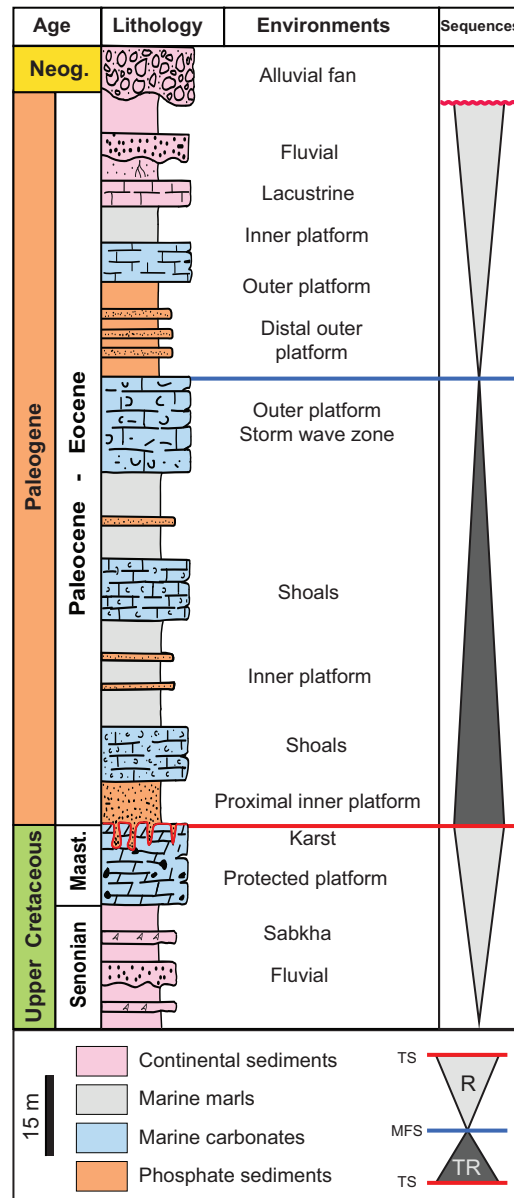

Fig. 2. Synthetic log of the Moroccan High Atlas phosphate-bearing series showing the

marine dominated character of the studied sedimentary successions. Depositional

sequences are from Chellaï et al. (1995). TR: Transgressive hemicycle; R: Regressive

hemicycle; TS: Transgressive surface; MFS: Maximum flooding surface.

visualize the evolution of the depositional environments. Biostratigraphic dating was based on nannofossil analysis. The sediments collected have been studied in the fraction of 2-30 μm, separated by the decantation method using 7% solution of H_2O_2. Smear-slides have been mounted with Canada balsam and analyzed at an Olympus transmitting light microscope, with 1200x magnification. The preservation was estimated by using the criteria proposed by Roth and Thierstein (1972), as follows: P = poor, severe dissolution, fragmentation and/or overgrowth; the specific identification is hindered up to 75%; M = moderate dissolution and/or overgrowth; the specific identification is hindered up to 25%; and G=good, little dissolution and/or overgrowth; diagnostic characteristics are preserved, the specimens could be identified to species level (up to 95%). Calcareous nannoplankton taxonomic identification follows Perch-Nielsen (1985) and Burnett (1998). Biostratigraphic zones NP are from Martini (1971).

4. Age of the series

The phosphate series of Morocco ranges from the Upper Cretaceous to Paleogene. However, the precise limits of the different stratigraphic intervals are still unclear. The correlations and sequence stratigraphic interpretations we develop in this study require a critical review of the biostratigraphy. The currently acknowledged age framework is mainly based on early biostratigraphic works in the 20th century (e.g., Moret, 1938; Arambourg, 1952). The leading paleontological works were carried out within the exploited phosphate basins (Ouled Abdoun and Ganntour), which contain remarkably rich vertebrates and invertebrates' faunas. Selachian fauna is the most studied (Arambourg, 1952; Cappetta, 1981, 1986, 1993; Noubhani and Cappetta, 1994; Noubhani, 2010; Cappetta et al., 2014). Other biostratigraphic studies were carried out

including, invertebrates (Salvan, 1954), dinoflagellates (Rauscher and Doubinger, 1982; Rauscher, 1985; Soncini, 1992), and pollens (Ollivier-Pierre, 1982). Hundreds of species have been discovered and compared to their European and North African equivalents. Following his pioneering paleontological study of vertebrates, Arambourg (1952) assumed that the phosphate series of Morocco extended from Maastrichtian to Lutetian and he defined three bio-units: Upper Cretaceous (Maastrichtian), Paleocene (Danian and Thanetian), and Eocene (Ypresian and Lutetian). Most of the subsequent studies focused more on the paleontological rather than stratigraphical consequences, and do not change significantly the bio-units defined by Arambourg (1952). More recently a chemostratigraphic approach, based on organic carbon isotopes, has been conducted within the Ouled Abdoun basin (Yans et al., 2014). The $\delta^{13}C_{org}$ data indicates the presence of the Selandian, a possible gap of the upper Thanetian, and supports the absence of Lutetian occurrence within the phosphate series of Ouled Abdoun.

The phosphate series of the High Atlas is by far less studied when compared to the exploited basins. The stratigraphic framework is based mainly on older works (Moret, 1938) and the identification of three mollusk fauna horizons within the Ouarzazate basin: Fauna A (Maastrichtian-Danian), Fauna C (Thanetian-Ypresian), and Fauna B (Ypresian-Lutetian). It can be noted that the inconsistent labeling of horizons has been a source of later misinterpretations. This work was completed by Roch (1939) and Gauthier (1960), who contributed to the recognition of the lower parts of the series (Maastrichtian and Danian) Arambourg (1937) defined the Lutetian in the upper parts of the series as he discovered *Carolia placunoïdes* within phosphatic marls. Selachian fauna was locally studied within the eastern part of the Ouarzazate basin and compared to its equivalent within the exploited basins (Cappetta et al., 1987; Gheerbrant et al., 1993; Tabuce et al.,

235   2005). Pollen and microplankton were also studied within the Upper Ypresian-Lower

236   Lutetian (Mohr and Fechner, 1986). A magnetostratigraphic approach has been

237   attempted in the eastern part of the Ouarzazate basin, suggesting much younger ages for

238   the series and attributing the lower red-beds, classically known as Senonian, to the

239   Thanetian-Danian (Gheerbrant et al., 1998).

240   The reliability of these biostratigraphic age determinations is questionable since facies

241   are frequently diachronous and the study of Selachian fauna was mostly interested in the

242   evolutionary trends of the species. The magnetostratigraphic results are not relevant

243   since the interpretation of magnetic reversal profiles was performed assuming two

244   different scenarios with constant sedimentation rates for the entire series.

245   As seen above, the age control of the studied sequence is poorly constrained in the

246   Maastrichtian to Eocene outcrops along the borders of the High Atlas. No

247   biostratigraphically significant macrofossils nor foraminifera were found in the marine

248   intervals so, we sampled Amizmiz and My Brahim sections for calcareous nannofossils.

249   Only some of the Amizmiz section samples yielded nannoflora (Fig. 3). Some of the

250   analyzed samples yielded more diversified and poorly to moderately preserved

251   nannofossils; the assemblages contain typical Paleocene to Lower Eocene nannofossils,

252   such as *Zygrhablithus kerabyi, Discoaster multiradiatus, Sphenolithus primus*, *S.*

253   *anarrhopus, Fasciculithus tympaniformis, F. hayii, Coccolithus pelagicus, Braarudosphaera*

254   *bigelowii, Heliolithus kleinpelli, Bomolithus bramlettei, Zeugrhabdotus sigmoides,* and

255   *Toweius* spp. No reworked nannofossils from older deposits have been encountered in

256   the identified assemblages.

The sample AMZ 10 contains rare specimens of *Fasciculithus tympaniformis, Coccolithus pelagicus, Zeugrhabdotus sigmoides, Toweius pertusus, Biscutum* sp. and *Thoracosphaera saxea*. The FO of *Toweius pertusus* (NP4 biozone) took place in the late Danian. In the assemblages, *Fasciculithus tympaniformis* is also present; the FO of the aforementioned species is placed towards the top of NP5 in the Selandian (Agnini et al., 2007). Hence, a late Danian to Selandian age may be assumed for this sample.
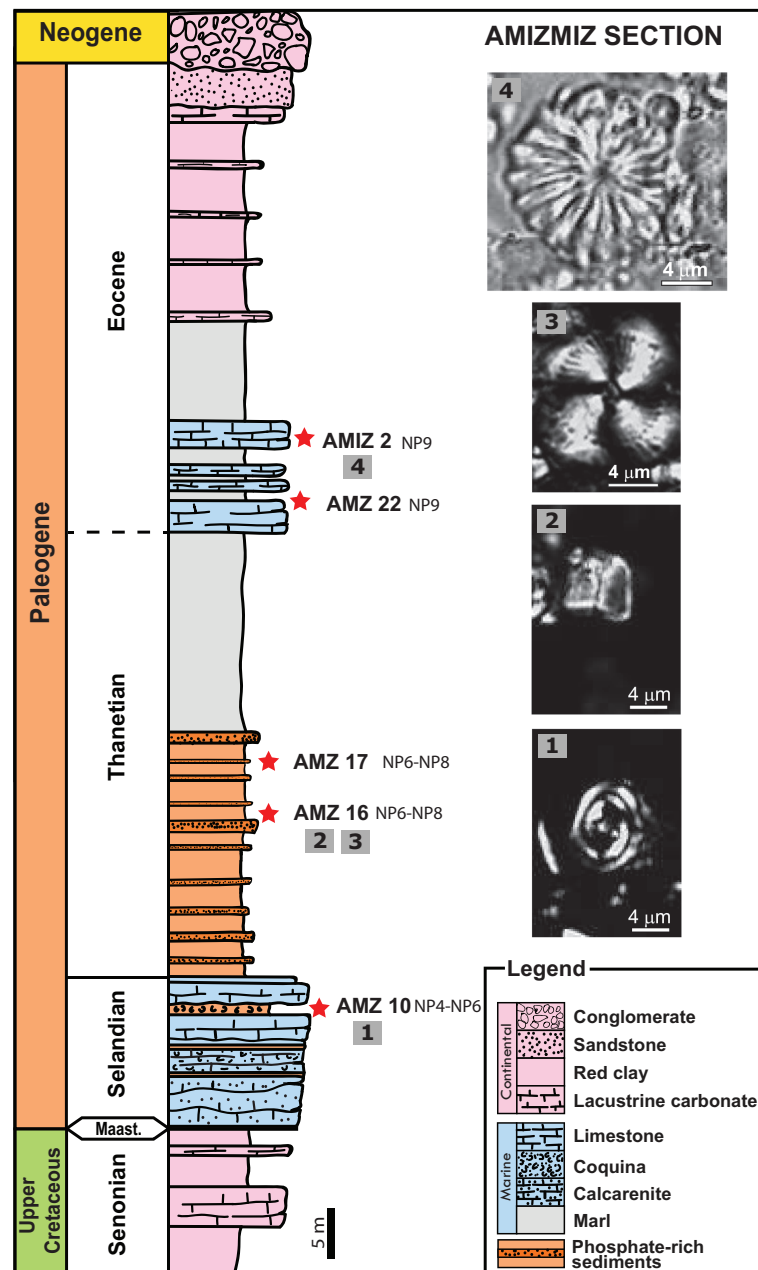
Fig. 3. Sedimentary log of the Amizmiz section with biostratigraphic samples containing nannofossils plotted in red stars. All the presented nannofossils are LM (light microscope) photomicrographs in N+ (crossed-nicols), except the nannofossil 4 observed in NII (polarized light). 1 – Zeugrhabdous sigmoides (Bramlette and Martini, 1964; Bown and Young, 1997); Sample AMZ 10. 2 – Fasciculithus tympaniformis (Hay and Mohler in Hay et al., 1967); Sample AMZ 16. 3 – Heliolithus kleinpellii; Sample AMZ 16. 4 – Discoaster multiradiatus (Bramlette and Riedel, 1954); Sample AMIZ 2.

An assemblage with *Heliolithus kleinpellii, Fasciculithus tympaniformis, Sphenolithus primus, Coccolithus pelagicus, Braarudosphaera bigelowii, Zeugrhabdotus sigmoides*, *Toweius* spp. and *Ellipsolithus macellus* was found in the sample AMZ 16. *Heliolithus kleinpellii* firstly occur towards the top of the NP6 biozone (Agnini et al., 2007). This bio-event, along with the presence of *Toweius* taxa, including *Toweius tovae*, are indicative of a late Selandian to Thanetian age (NP6-NP8 biozones). A similar age was recorded in the sample AMZ 17. The occurrence of *Discoaster multiradiatus* in the samples AMZ 22 and AMIZ 2 indicates the presence of NP9 biozone (Agnini et al., 2007), late Thanetian in age.

Our new biostratigraphic data suggest an older age than previously established for the phosphate accumulation in the High Atlas area. The upper phosphate-rich interval spans the entire Paleocene, over a 10 My period.

5. Facies analysis

The studied sections consist of carbonate-dominated sediments containing significant phosphate accumulations. Detailed field and microscopic observations of the investigated sedimentary successions allowed the identification 26 facies, interpreted in

297   terms of sedimentary processes and depositional environments, providing clues about

298   paleobathymetry and helping to trace the relative sea-level variations curve. Genetically-

299   related facies were grouped into six facies associations (FA) defining depositional

300   environments. Facies associations are summarized in table 1.

Facies association	Description	Interpretation
FA1	Coarsening upward successions; medium-grained sandstone with steep cross-bedding sets; thick evaporitic red-beds; parallel horizontally-laminated chalky limestones with *Charophyta* and *Ostracods*; carbonate concretions and glaebules with roots traces; planar cross-stratified fine-grained sandstone; matrix-supported polygenic conglomerates (Fig. 4A-F).	Alluvial plain environment Debris flow Fluvial unidirectional currents Aeolian dune migration Lakes and evaporitic sabkha
FA2	Thick successions of interbedded grey marls and carbonates; mudstone to wackestone textures, horizontal parallel laminations, *Thalassinoides* bioturbation, poorly diversified fauna with relatively well-preserved thin shells of bivalves and gastropods (Fig. 4G-M).	Protected platform Suspension fallout
FA3	Geometrically irregular and discontinuous sedimentary bodies; coquina beds with fragmented shells of oysters and gastropods; cross-bedded calcarenites and phosphatic sandstones (Fig. 4N-P).	Open inner platform Shoal, wave reworking
FA4	Carbonate and sandy material; packstone to grainstone textures; diversified fauna including *Nautiloid*s, echinoids, oysters, and scarce foraminifera; *Thalassinoides* bioturbation; bed amalgamation and hummocky cross stratifications (Fig. 5A-F).	Outer platform between fair-weather wave-base and storm wave-base
FA5	Muddy carbonate; parallel thinly-laminated phosphatic marls; granular phosphate beds with densely packed peloids; climbing ripples; micro-hummocky cross stratification; *Nautiloids*; *Thalassinoides* burrows (Fig. 5G-J).	Around the storm wave base, storm winnowing of phosphate
FA6	Fine dark muddy organic-rich levels intercalated with normally graded sandstones to conglomerates, composed of a mixture of phosphatic and detrital particles (Fig. 5K-L).	Offshore suspension fallout episodically interrupted by gravity flows.

301   Table 1: Summary of facies associations in the Upper Cretaceous-Paleogene phosphate

302   series of the Moroccan High Atlas.

303

FA1. Alluvial plain

Description:

This facies association is well exposed across the investigated zones. It systematically bounds the carbonate intervals of the sections. FA1 is organized in coarsening and thickening-upward succession in the uppermost parts of the sections, while it shows finning-upward trend in the lower parts. FA1 includes cross-laminated sandstones (F1), matrix-supported conglomerates (F2), evaporitic red-beds (F3), planar cross-stratified sandstones (F4), ostracod and charophyta chalky limestones (F5), and carbonate concretions and glaebules (F6).

F1 is preserved locally within Ouarzazate basin. It corresponds to m-scale intervals of medium-grained, very well-sorted yellow sandstone composed of round and mat grains of quartz. This poorly consolidated facies is azoic and shows m-scale cross-bedding sets, where cm-sized steep foreset laminae are curved and become tangential to the basal surface of the dunes (Fig. 4A). F2 consists of m-scale (up to 10 m) bars of matrix-supported conglomerate composed of very poorly-sorted, weakly organized, pebble to cobble-grade sub-angular to sub-rounded polygenic clasts within reddish mud to sand matrix (Fig. 4B-C). F3 is composed of m-scale banks of fine-grained, very well-sorted, azoic, red-colored sandstone showing planar cross-stratification. F4 corresponds to poorly consolidated, structureless, azoic red clay and silt, interbedded with slightly deformed gypsum beds (Fig. 4D). The bedding planes are rarely visible, and are mostly highlighted by gypsum levels (Fig. 4D). In this facies, no root traces or concretions were found. F5 comprises cm to m-thick beds of thinly-laminated, white spongy limestone with sharp planar lower and upper contacts, containing ostracods, charophyta, and few thin-shells of bivalves. F6 consists of m-scale horizons of yellow/white, cm-sized,

16

328   structureless carbonate concretions and glaebules (Fig. 4E), with root traces and

329   brecciated aspect. Observed glaebules consist of spherical carbonate peloids (<2 cm)

330   surrounded by circumgranular cracks (Wright, 1994)(Fig. 4F).

331   *Interpretation*

332   In F1, the rounded morphology of quartz grains and their mat aspect suggest an

333   important abrasion by grain collision during wind transport (Krinsley and Trusty, 1985;

334   Pye and Tsoar, 2009). The steep geometry of the foreset laminae indicates sedimentation

335   by aeolian dune migration (Hunter, 1977; Kocurek, 1991; Posamentier and Walker, 2006;

336   Pye and Tsoar, 2009). In F2, the matrix-supported conglomerates with their chaotic

337   character and randomly-oriented clasts indicate cohesive subaerial debris-flow

338   sedimentation (Nemec and Steel, 1984; Major, 2003), taking place in an alluvial fan

339   setting, at the border of the alluvial plain (Blair and McPhe, 1994). In F3, the oxidation

340   color, planar cross-stratification, and fine-grained aspect argue for a fluvial origin of this

341   facies, interpreted to form under lower-flow regime by unidirectional currents (Miall,

342   1996). In F4, the interbedding pattern of red clay and gypsum, as well as the absence of

343   pedogenesis evidence in this facies suggest formation under evaporitic conditions of

344   sabkha (Glennie, 1970), developed under hot and arid climate (Algouti et al., 1999). In F5,

345   the muddy depositional texture and fine parallel laminations indicate deposition under

346   low-energy conditions. The presence of ostracods and charophyta allows to assign this

347   facies to the lacustrine/palustrine domain (Murphy and Wilkinson, 1980; Platt and

348   Wright, 1991). In F6, carbonate concretions and glaebules with root traces and brecciated

349   aspect are distinctive features of paleosol horizons developed on a carbonate host rock

350   (Freytet and Plaziat, 1982; Freytet and Verrecchia, 1989; Wright, 1994). The observed

circumgranular cracks result from desiccation of the host rock, and confirm the pedogenic origin of these horizons (Wright, 1994).

FA2. Restricted inner platform

Description:

This facies association is represented in all sections by carbonate sediments, organized in marl-limestone alternations. FA2 includes grey laminated marls (F7), horizontally-laminated dolo-mudstones (F8), *Turritella* and bivalves wackestones/packstones (F9), and bioturbated phospharudites (F10).

F7 corresponds to poorly consolidated m-scale intervals of horizontally to wavy-laminated grey marls (Fig. 4G), lacking macrofossils and bioturbation activity, it may contain chert nodules. This facies is interbedded with mudstone and wackestone beds. F8 is composed of cm to m-thick beds of horizontally-laminated yellow/white dolomitic mudstones to wackestones (Fig. 4H), containing preserved thin shells of gastropods and bivalves, scattered small sub-angular quartz grains, and rhombohedral dolomite crystals. The lower surface of this facies shows occasionally *Thalassinoides* burrows network (Fig. 4I). F8 is sometimes affected by strong pervasive silicification and karstification filled with red silt material (Fig. 4J). F9 includes m-thick bars of white-colored bioclastic limestones with wackestone to packstone textures. It contains relatively well-preserved, small-sized *Turritella* gastropods and bivalves. This facies exhibits low angle cross-beds (Fig. 4K), and locally shows few scattered nautiloids (Fig. 4L), as well as intense pholad borings at its upper surface (Fig. 4M). F10 consists of m-scale intervals of friable, moderately-sorted phospharudite, containing yellow/brown color fragmented and agglomerated peloids (up to 5 mm), fish teeth, and lithoclasts in a carbonate matrix. This

18

374   facies infills and overlays karstic cavities, and exhibits at its upper part, *Thalassinoides*

375   burrows infilled by gravel-sized phosphate grains.

376   *Interpretation*

377   The observed laminations in F7 suggest sedimentation by suspension fallout from

378   relatively quiet shallow-water (Flügel, 2010). Locally observed wavy-laminations are

379   generated by the wind-driven motion of the water column. In F8, horizontal laminations,

380   fine texture, and preserved poorly diversified fossil shells suggest formation in low-

381   energy environment within the inner platform (Flügel, 2010). The bioturbation style in

382   this facies is indicative of a shallow water environment (Ekdale and Bromley, 1984) and

383   a low sedimentation rate (Ekdale and Bromley, 2003). The small-sized and poorly

384   diversified fauna in F9 indicate deposition in the inner parts of the platform. Nautiloids

385   are indicative of open marine environments (Frey, 1987), their presence in this facies can

386   be explained by storm wash-over transport to the inner platform, which is also supported

387   by the presence of low-angle cross-beds. Nevertheless, this facies can also form within an

388   open shelf lagoon. In F10, the fragmented and agglomerated character of phosphatic

389   grains suggest significant transport and reworking. The presence of this facies within

390   karstic cavities allows to interpret it as allochthonous phosphate transported landward

391   during early transgression. This facies continued to accumulate above karsts in a shallow

392   water environment, where trace fossils were present.

393   **FA3. Inner platform (shoreface)**

394   *Description:*

395   This facies association is exposed discontinuously within the studied zone. It consists

396   predominantly of granular carbonates and shell beds organized in alternations and

397   exhibiting geometrically irregular bodies (Fig. 4N). To the west, in the Erguita section,

398   this association contains more sandy material. FA3 comprises calcarenites (F11), coquina

399   beds (F12), phosphatic sandstones (F13), and wavy-laminated sandstones (F14).

400   F11 consists of m-thick geometrically irregular levels of well-sorted granular limestones,

401   containing well-rounded quartz grains (Fig. 4O), cm-sized lithoclasts and bioclastic

402   debris (mostly fragmented oysters), and occasionally exhibiting trochoidal ripples and

403   cross-bedding. F12 corresponds to massive bars with scoured bases of bioclastic

404   limestone, showing a massive shell concentration, including disarticulated bivalves and

405   fragmented gastropod shells (Fig. 4P). In some cases, oyster fragments dominate the shell

406   content. F13 consists of indurated beds (<1.5 m) of relatively well-sorted, medium-

407   grained, locally cross-bedded grey phosphatic sandstone. This facies contains diversified

408   phosphatic particles (peloids, coprolites, fish teeth, and bone and vertebrate fragments)

409   and detrital grains dominated by sub-angular quartz. F14 consists of well-sorted, fine-

410   grained, wave-rippled calcareous sandstone, containing significant amount of detrital

411   quartz grains and few phosphatic particles.

412   *Interpretation:*

413   The nature and grain size of F11 bears evidence of reworking of an unlithified carbonate

414   material leading to the formation of a calcarenite. The rounded aspect of quartz grains

415   suggests an important wave-reworking of the sediment, which is also supported by the

416   presence wave ripples. The irregular geometry of these sediments, as well as the high-

417   energy character they display allows to interpret this facies as shoal accumulation. In F12,

418   the fragmented fossil shells indicate accumulation within high-energy domain, where

419   winnowing and reworking dynamics concentrate shells by the removal of the siliciclastic

420 fine detritus (Kidwell, 1986; Fürsich and Oschmann, 1993; Jahnert et al., 2012; Fick et al.,

421 2018). The significant presence of sub-angular quartz grains in F13 reflects the vicinity

422 of detrital source. We interpret this facies to have accumulated within the inner platform

423 zones subjected to wave action, which explains the presence of cross-bedding. In F14, the

424 grain size and sorting, along with the presence of wave ripples indicate that this facies

425 accumulated within the inner platform above the fair-weather wave-base (Burchette and

426 Wright, 1992).

427

Fig. 4. Facies and facies associations (FA1-FA3). (A) Cross-bedded sandstone. (B, C) Matrix-supported conglomerate with randomly organized clasts (white triangles). (D) Red-beds and gypsum alternations (black triangles). (E) Carbonate paleosol. (F) Light-colored glaebules (black arrows) surrounded by grey-colored circumgranular cracks. (G) Grey marls. (H) Horizontally-laminated dolomitic mudstones. (I) Lower surface of a

446   dolomudstone bed showing Thalassinoides burrows. (J) Silicified and karstified

447   dolomitic mudstone. (K) Packstone showing low-angle cross-beds. (L) Turritella and

448   bivalves packstone containing nautiloids. (M) Intense pholad borings (black arrows) at

449   the upper surface of F9. (N) Panoramic view of the My Brahim section. (O) Granular

450   limestone with quartz grains (black arrows). (P) Fragmented fossil shells coquina. pho:

451   pholad; qtz: quartz.

452   **FA4. Outer platform (lower shoreface)**

453   *Description:*

454   This facies association is well-developed in the surveyed zones, except in the far east of

455   the Ouarzazate basin. FA4 is mainly composed of carbonate successions turning into

456   sandy facies towards the Erguita section. FA4 is made up of carbonate-matrix

457   conglomerates (F15), oyster marls (F16), *Cardita* grainstones (F17), *Thersitae* limestones

458   (F18), echinoid bioturbated limestones (F19), and hummocky cross-stratified calcareous

459   sandstones (F20).

460   F15 consists of sharp-based beds of poorly sorted conglomerate with carbonate matrix,

461   supporting dark-brown sub-rounded siliceous pebbles, cm-sized carbonate lithoclasts,

462   oyster and gastropod fragments, and few dark brown phosphate grains (Fig. 5A). F16

463   corresponds to m-scale intervals of structureless grey marls containing massive

464   accumulation of well-preserved uniform cm-sized oysters and showing no signs of

465   bioturbation. F17 consists of 1 m-thick grainstone beds containing moderately preserved

466   *Cardita*, oysters, recrystallized thick-shell gastropods, siliceous pebbles, and phosphate

467   peloids. F18 is made up of m-scale packstone bars containing disarticulated bivalves,

468   recrystallized thick-shell gastropods (*Hemithersitae marocana*) (Fig. 5B), nautiloids,

23

469   scarce benthic foraminifera, echinoids, quartz grains (Fig. 5C), and carbonate lithoclasts.

470   F19 comprises 3 to 5 m-thick recrystallized, bioturbated, and amalgamated bioclastic

471   packstone beds containing uniform cm-sized echinoids (Fig. 5D), bivalves, scare

472   foraminifera, carbonate lithoclasts and phosphate particles (Fig. 5E). F20 consists of well-

473   sorted, fine to medium-grained calcareous sandstone, exhibiting hummocky cross-

474   stratification (Fig. 5F).

475   *Interpretation:*

476   The nature and organization of clasts indicate that F15 corresponds to an

477   intraformational conglomerate formed by storm reworking of semi-consolidated

478   sediments in the outer platform zone (Dott Jr, 1974). F16 is interpreted to form by in-situ

479   growth and accumulation of monospecific fauna on open muddy shelf. In F17, the

480   grainstone texture and the predominance of thick fossil shells suggest sedimentation

481   within agitated environment of the outer platform. The presence of nautiloids and

482   echinoids in F18 argues for an open marine environment (Frey, 1987; Bachmann and

483   Hirsch, 2006), which is subjected to storm reworking, as suggested by the fragmentation

484   of the thick fossil shells. In F19, the ubiquity of echinoids indicates sedimentation under

485   open marine conditions (Bachmann and Hirsch, 2006), where bed amalgamation is

486   interpreted to form by storms (Cheel and Leckie, 1993). F20 exhibits characteristics of

487   storm-generated deposits as evidenced by the presence of hummocky cross-stratification

488   (Cheel and Leckie, 1993). It is interpreted to form within the outer platform between the

489   fair-weather wave-base and the storm wave-base (Burchette and Wright, 1992).

490   **FA5. Outer platform (offshore transition)**

491   *Description:*

492 This facies association overlies FA4 and consists of carbonate and phosphate-dominated

493 sediments organized in alternations. FA5 comprises micro-HCS sandstones (F21),

494 nautiloids bioturbated mudstones (F22), granular phosphates (F23), and phosphatic

495 marls (F24). As the previous facies association, FA5 shows more sandy material within

496 the Erguita section.

497 F21 consists of cm to m-thick beds of fine to medium-grained, well-sorted calcareous

498 sandstone composed mainly of quartz grains and few phosphatic particles, including

499 peloids, lithoclasts, and bone fragments. This facies exhibits micro-hummocky cross-

500 stratification overlying well preserved centimetric climbing ripples (Fig. 5G). F22 is

501 composed of cm to m-thick beds of moderately bioturbated mudstones to wackestones

502 (Fig. 5H), with sharp upper and lower contacts. This facies contains large well-preserved

503 nautiloids (Fig. 5I), some bivalves, phosphate grains, bone fragments, and fish teeth. F23

504 is made up of m-thick (up to 1 m) semi-consolidated beds of granular phosphate,

505 interbedded with phosphatic marls, and composed predominantly of well-sorted,

506 homogeneous, brown-honey, phosphatic peloids cemented by calcite and phosphate.

507 This facies contains also fish teeth and bone fragments. F24 corresponds to parallel

508 thinly-laminated, unconsolidated grey phosphatic marls (Fig. 5J), containing floating

509 peloids in a micritic matrix. This facies shows no evidence of bioturbation, and lacks

510 quartz and other detrital grains.

511 *Interpretation:*

512 In F21, the fine-grained character and the good sorting of the sediment suggest

513 deposition under low to moderate-energy. The presence of climbing ripples and micro-

514 hummocky cross-stratification indicates sedimentation within the offshore transition

515   under storm and temporary wave reworking (Dott and Bourgeois, 1982). The fine texture

516   and *Thalassinoides* bioturbation of F22 indicate deposition under low-energy conditions

517   from mud settling. Given the presence of large nautiloids, we interpret this facies to form

518   in the outer platform below the storm wave-base (Frey, 1987). The granular feature of

519   F23 and its presence, sandwiched within phosphatic marls suggest hydrodynamic

520   accumulation around the storm wave-base from previously pristine phosphate facies

521   (Pufahl and Groat, 2017). In F24, the parallel lamination and the fine texture suggest

522   sedimentation under low-energy conditions from the fallout of particles in suspension.

523   The absence of coarse-grained detritals indicates deposition in distal parts of the

524   platform below the storm wave-base, where phosphatic peloids formed by authigenesis

525   (Föllmi, 1996).

526   **FA6. Basin (offshore)**

527   *Description:*

528   This facies association exclusively occurs within the Erguita region. It is organized in

529   alternations between normally-graded microconglomerates (F25) and organic-rich

530   muds (F26). FA6 constitutes the ultimate part of a fining upward sequence. F25

531   comprises cm to m-thick sharp-based beds of normally graded sandstone to micro-

532   conglomerate (Fig. 5K). This facies contains detrital grains, phosphate particles, fish

533   teeth, bone fragments. F26 consists of thin layers (20 cm) of dark-colored muddy fine

534   sediment showing no internal structure and lacking bioturbation (Fig. 5L). This facies

535   occur by progressive an continuous transition from upper offshore sediments.

536   *Interpretation:*

The normally-graded sandstones and microconglomerates, occurring in association with organic-rich beds, are interpreted as disruption episodes caused by gravity-driven currents transferring detrital material and phosphate particles from shallow to deeper water environment (Pickering et al., 1986). The accumulation of this facies occurs by rapid grain by grain deposition (Pickering et al., 1986). The absence of hydrodynamic structures and the fine-grained aspect of the organic-rich facies indicate deposition under a low-energy regime, from the settling of suspension particles in a distal offshore environment (Stow et al., 2001). In this setting, anoxia conditions favor the preservation of the organic matter.
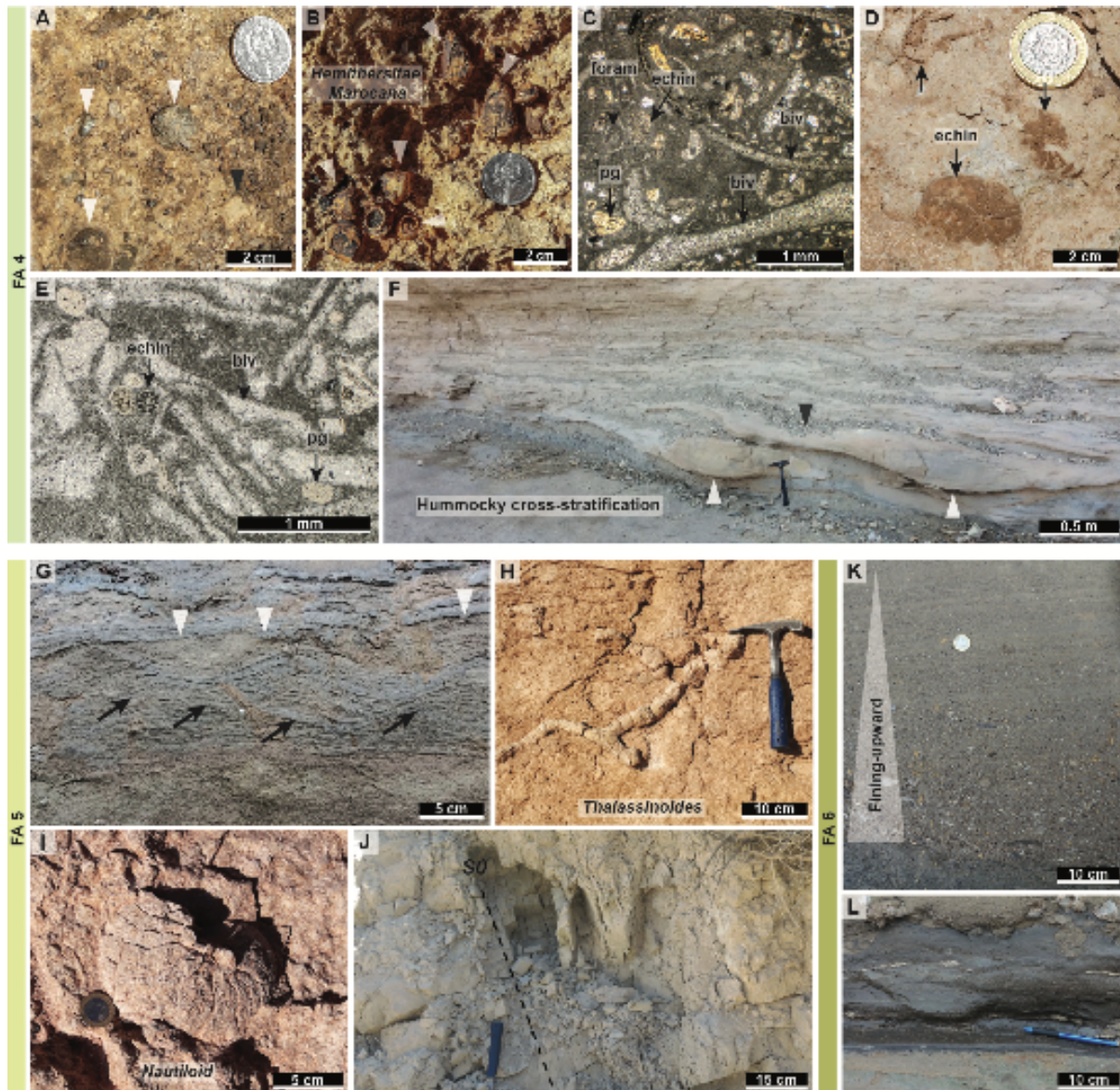
556 Fig. 5. Facies and facies associations (FA4-FA6). (A) Carbonate matrix-supported

557 conglomerate, containing siliceous pebbles and carbonate lithoclasts (white triangles).

558 (B) Thersitae limestone. (C) Transmitted light photomicrograph of a Thersitae limestone.

559 (D) Echinoid limestone. (E) Transmitted light photomicrograph of an echinoid limestone.

560 (F) Calcareous sandstones showing hummocky cross-stratification. (G) Slightly

561 phosphatic sandstone, showing climbing ripples (black arrows), and micro-hummocky

562 cross-stratification (erosion surface highlighted with white triangles). (H, I) Nautiloids

563 mudstone showing Thalassinoides burrows. (J) Parallel thinly-laminated phosphatic

564 marls. (K) Normally graded sandstone. (L) Muddy organic-rich fine sediment. biv:

565 bivalve; echin: echinoid; foram: foraminifera; pg: phosphatic grain; qtz: quartz.

566 6. Depositional model

567 The aforedescribed facies associations are genetically related and show continuous

568 lateral shifting, during the studied Late Cretaceous to Paleocene interval. The overall

569 dominance of carbonate, the fossil content, sedimentary structures, and facies

570 distribution, suggest a depositional model of a shallow-water carbonate platform,

571 characterized by tectonic quiescence and unequally distributed clastic inputs (Wilson,

572 1975; Burchette and Wright, 1992) (Fig. 6). Proximal facies are located in the east and

573 they change westward to more distal facies. This is mirrored by westward thickening of

574 the sedimentary sequences. In addition, a distinct orthogonal (southwards) facies

575 evolution trend is documented. The sedimentary configuration changes from shallow

576 water carbonate platform in the proximal area to mixed carbonate and siliciclastic storm-

577 dominated platform, in the Souss basin (Erguita section, Fig. 6). Similarly, this is

578   accompanied by an important southward thickening of the sequences and the presence

579   of more siliciclastic inputs, including gravity flows.

580   In this general setting, the proximal continental parts correspond to an array of alluvial

581   plain sub-environments, ranging from aeolian to lacustrine. The inner platform zone

582   shows low-energy muddy carbonates, locally interrupted by storm events. Shoal bodies,

583   acting as local and discontinuous barriers, exhibit high-energy granular and shelly

584   carbonate facies developed under wave reworking conditions. The outer platform

585   comprises various facies recording different energy degrees as a function of the storm

586   wave-base position and exhibits typical storm-derived structures, mainly hummocky

587   cross-stratification. Distal parts correspond to the basin zone with typically low-energy

588   organic-rich sediments disrupted by turbiditic events.

589

590

591

592
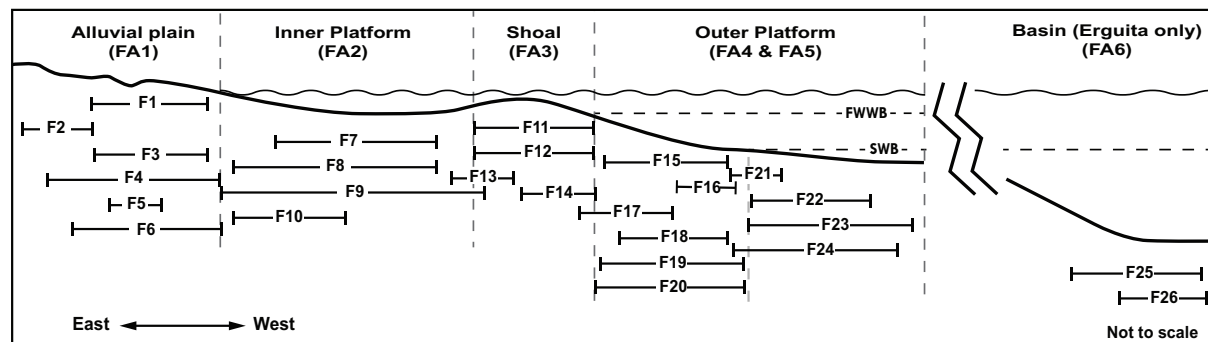
593   Fig. 6. 2D facies substitution diagram of the studied sedimentary series highlighting the

594   distribution of the defined facies within a shallow-marine platform profile. FWWB: fair-

595   weather wave-base; SWB: storm wave-base.

29

7. The different types of the phosphate-rich sediments of the High Atlas

The petrography of the phosphatic sediments was extensively studied due to their economic importance. Consequently, many classifications have been proposed to explain the diversity of phosphate lithofacies. The most common nomenclature is based on the modified Dunham/Embry and Klovan classifications (Trappe, 2001) by studying the relative proportions between phosphatic and non-phosphatic allochems, and matrix (Slansky, 1986; Trappe, 2001). In the Moroccan phosphate series, the petrography of the phosphatic sediments is well established. The phosphatic allochems were studied based on grain shape, size, internal structure, and origin (Mouflih, 2015). In this study, we describe the different phosphate lithofacies with respect to the sedimentary processes involved in their formation and accumulation. Correspondingly, five different phosphate types are described and categorized into transported and non-transported facies with respect to the primary phosphogenesis zone (Table 2).

Key Features	Pristine phosphate	Winnowed and reworked phosphate			
		In-situ	Transported		
			Platform	Basin	Karst
Lithology	Phosphatic marls	Granular peloidal phosphates	Phosphatic sandstones & coquina	Phosphatic sandstones and microconglomerates	Microconglomerates and phospharudites
Bedding	Thin	Thick	Thick	Thin to thick	undefined
Thickness	5-30 m	0.1-1 m	0.1-1 m	0.1-2 m	2-10 m
Petrographic composition	Yellow-brown peloids Traces of organic matter Calcite	Densely-packed peloids, coprolites, vertebrate debris, fish teeth Calcite & phosphate cement	Peloids, coprolites, vertebrate debris, fish teeth, composite grains, quartz grains	Peloids, coprolites, vertebrate debris, fish teeth, composite grains, quartz grains	Agglomerated peloids Fish teeth Coprolites Quartz grains
Coarse detrital fraction	Absent or rare	Absent or rare	Very frequent	Frequent	Frequent
Sedimentary structures & depositional features	Horizontally laminated	Well-sorted Poorly consolidated	Well-consolidated Well sorted Cross-stratified	Normally graded	Unconsolidated Wavy laminated
Biological activity	Unbioturbated	Rarely bioturbated	Moderately bioturbated	Rarely bioturbated	Bioturbated *Thalassinoides* burrows
Process	Particles settling and francolite authigenesis	Storm and bottom currents winnowing	Transport and wave reworking	Gravity-driven transport	Wave currents transport and reworking
Phosphorus content	Low	High	Low to Medium	Medium	Medium to High
Sequence stratigraphic position	The base of the regressive system of a T-R sequence	The base of the regressive system of a T-R sequence	Occur in both stages of a T-R sequence	Around the distal maximum flooding zone	The base of the transgressive hemicycle
Spatial distribution	Northern border of the Marrakesh High Atlas	Northern border of the Marrakesh High Atlas	Abundant in the northern border of the Marrakesh High Atlas	Souss basin	Ouarzazate basin

Table 2: The main characteristics of the different phosphate lithofacies of the High Atlas.

31

6.1. Pristine phosphate

Description:

This phosphatic lithofacies is geographically restricted to the northern border of the Marrakesh High Atlas, and systematically occurs above FA4, which is capped by a hardground surface. Pristine phosphate facies consists of m-scale intervals of grey thinly parallel-laminated, poorly-consolidated phosphatic marls (Fig. 7A1), which prevents preparation of sample thin sections. It is composed of mm-sized homogeneous and structureless phosphatic grains scattered within a micritic matrix (Fig. 7A2). It is of interest to note that all the phosphatic allochems in this facies correspond to peloids (Fig. 7A2). This phosphate type shows no signs of bioturbation and a distinctive lack of detrital quartz grains.

Interpretation:

The fine depositional texture and the horizontal laminations fabric indicate deposition under a low-energy setting from the fallout of particles in suspension. The presence of phosphate peloids and the scarcity of detrital particles suggest the formation in relatively distal parts of the platform away from terrigenous inputs. Hence, we interpret these phosphatic marls to have formed pristinely in the outer platform, below the storm wave-base, where phosphatic peloids were precipitated authigenically in pore water microsystems at the water-sediment interface (Föllmi, 1996; Glenn et al., 1994; Pufahl et al., 2003; Pufahl and Groat, 2017; Soudry et al., 2013; Zhang et al., 2019). This phosphogenesis process requires the conjunction of many biochemical conditions to occur, including: i) the availability of phosphorus and its release from the organic matter

33

to pore water by bacterial mediation (Diaz et al., 2008; Krajewski et al., 1994), ii) the availability of fluorine (F), and iii) the pumping of Mg from pore water in order to precipitate the francolite by supersaturation of P (Jarvis et al., 1994, Glenn 1994).

6.2. Winnowed phosphate

Description:

This phosphatic facies only occurs along the northern border of the Marrakesh High Atlas, in close association with the previously described phosphatic marls, with which it is interbedded at a 0.1 to 1 m frequency (Fig. 7B1) over intervals that can reach a thickness of 30 m. This granular phosphate corresponds to a greyish, well-sorted, medium-grained, consolidated to semi-consolidated phosphate beds (Fig. 7B1). The cm to m-thick beds are almost entirely composed of densely-packed mm-sized rounded and structureless honey-brown peloids (Fig. 7B2-3). Beds also contain few vertebrate fragments and fish teeth showing generally elongated shapes. These particles are cemented by calcite and phosphate (Fig. 7B3). The morphology of grains is similar to pristine grains and show no signs of transport or grain overgrowth. This phosphatic facies has yielded the highest phosphorus concentrations (up to 25% P_2O_5) with respect to the other phosphate types in the studied sections.

Interpretation:

The composition, granular texture, and the very good sorting indicate a high-energy setting of this lithofacies. The interbedding pattern between granular phosphate and phosphatic marls suggests their genetic link. Similar interbedding pattern was described within the Campanian phosphorite of Jordan (Pufahl et al., 2003). We interpret the

granular phosphate to form around the storm wave-base where bottom water currents sweep the pristine phosphate sediment to remove the fine muddy fraction and concentrate peloids (Pufahl and Groat, 2017). This concentration process by winnowing is enhanced by the specific gravity of francolite, which is higher (2.9 g/cm3) than other sediment particles (1.5 to 2.5 g/cm3; (Föllmi, 1996; Pufahl and Grimm, 2003). The peloids in this facies are cemented by phosphate, which indicates that a second phosphatization phase occurred, as the winnowed phosphate is reburied into the phosphogenesis zone (Glenn et al., 1994). The winnowing process therefore plays a critical role in the enrichment of the primary phosphate accumulation. The replication of this process over wide areas is thought to be responsible for the world's major economic phosphate deposits (Glenn et al., 1994; Föllmi, 1996; Pufahl and Grimm, 2003; Pufahl and Groat, 2017).
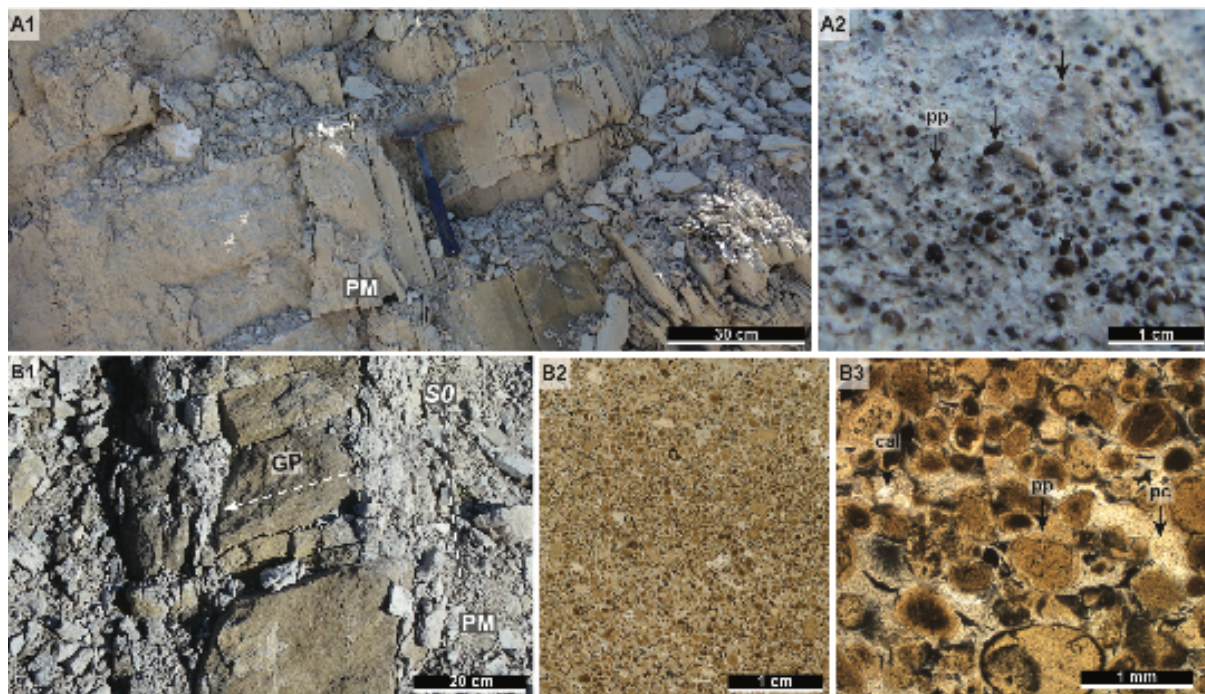
Fig. 7. In-situ formed phosphate lithofacies of the High Atlas. (A1) Pristine thinly parallel-laminated phosphatic marls. (A2) Limestone marl containing pristine phosphatic peloids.

35

(B1) Granular phosphate bed intercalated within phosphatic marls. (B2) Densely-packed peloids in granular phosphate. (B3) Transmitted light photomicrograph showing the composition of granular phosphate lithofacies. PM: phosphatic marls; GP: granular phosphate S0: stratification plane, pp: peloid; pc: phosphatic cement; cal: calcite.

6.3. Phosphatic lags

Description:

This phosphatic lithofacies is identified in different sections and at different stratigraphic positions. It occurs as phosphatic sandstones, with sharp upper and lower contacts (Fig. 8A1), or as cross-bedded phosphatic coquina. This facies is associated with the FA3. Phosphatic lags are made up of a mixture of relatively well-sorted phosphatic and non-phosphatic grains (Fig. 8A2). The phosphatic grains consist of yellow-brown well-rounded mostly structureless peloids, rod-shaped coprolites, fish teeth, bone fragments, and bioclasts (Fig. 8A2-3). Unlike the previous types, these phosphate sediments contain a significant amount of sub-angular quartz grains (Fig. 8A2) and other terrigenous components, including cm-sized pebbles.

Interpretation:

The lithology, the composition and the sedimentary structures recorded within this phosphate type suggest a formation under high-energy conditions enhancing the reworking and sorting of sediments. The ubiquity of sub-angular to sub-rounded quartz grains suggests the vicinity of proximal detrital supply. These conditions are common to the shoal zone within the wave action zone of a shallow-water platform. Storm and wave currents transport the phosphate grains, initially formed in situ, to the inner parts of the

platform, where they are mixed with a significant proportion of detrital components, and reworked by waves (Trappe, 1998). The accumulation of this phosphate type in a close association with shoal bodies suggests that these bodies play a role in trapping the reworked phosphate particles within the sheltered back-shoal depressions.

6.4. Karst-filling phosphate

Description

This phosphate facies occurs locally, within the Ouarzazate basin. It consists of up to 5 m thick phosphate sediment filling and covering karstic pockets (Fig. 8B1-2). This phosphate lithofacies exhibits a fining-upward trend above the karstic surface, within the cavities. It passes upward to beds displaying *Thalassinoides* burrows filled with granule-sized phosphatic grains (Fig. 8B3), and calcic geodes. These karstic pockets consist of several cm-wide cavities developed on carbonate rocks and can reach a depth of several meters. This phosphatic lithofacies corresponds to an unconsolidated phospharudite composed of very-coarse to granule-grained, medium sorted phosphatic grains contained in a grey carbonate matrix (Fig. 8B4). Petrographically, phosphate grains consist of agglomerated peloids (Fig. 8B4). A single peloid corresponds to a rounded yellow to dark brown grain. Phosphatic grains are mostly structureless and show evidence of corrosion (Fig. 8B4-5). They are frequently very fractured and altered (Fig. 8B5). The non-phosphatic grains consist of lithoclasts and few detrital particles.

Interpretation:

The lithology and the composition suggest a marine origin of this lithofacies. This phosphate lithofacies is interpreted as an allochthonous sediment, whose accumulation

onset corresponds to an early stage of a transgression above an emerged and karstified carbonate platform, where previous phosphate lithofacies were transported landwards. The agglomeration, corrosion, fragmentation, and alteration of phosphatic grains indicate significant transport and reworking of sediments. We interpret this accumulation to occur in two steps: i) landwards currents transport previously pristine and winnowed phosphate to inner parts of the platform; ii) during transgressive events, as the shoreline shifts landward, reworked phosphate sediments are eroded and further transported landward to cover previously exposed karstified sediment. This process occurs in the absence of significant detrital inputs, which explains the relatively good ore-grade of this phosphate type. This type of accumulation has been reported from the Upper Cretaceous phosphorite of Eshidiyya in Jordan containing friable phosphorite accumulations within a karstic depression (Abed et al., 2007).

6.5. Turbiditic phosphate

Description

This phosphate type occurs locally within the Erguita section, in the southwest of the study area, where it is associated with deeper environments facies represented by organic-rich layers (F26). It corresponds to coarse-grained to very coarse-grained and normally graded beds (Fig. 8C1) containing a wide variety of phosphatic particles including peloids, bone fragments, fish teeth, and non-phosphatic particles comprising carbonate lithoclasts and detrital grains (Fig. 8C2).

Interpretation:

The normal grading pattern and the association with offshore sediments suggest deposition in distal environments under turbidity conditions. We interpret this phosphate lithofacies as a gravity-flow deposit, with rapid accumulation of sediments enhancing the normal grading pattern. The phosphatic particles were derived from the other phosphate lithofacies, which have been transported basinwards. This interpretation corroborates with previous studies where this phosphate accumulation mode of phosphate was reported from many world-class phosphate deposits such as in Baja California in Mexico (Galli-Olivier et al., 1990), in the Upper Cretaceous of Colombia, (Föllmi et al., 1992), or in the Miocene of Salento in Italy (Föllmi et al., 2015).
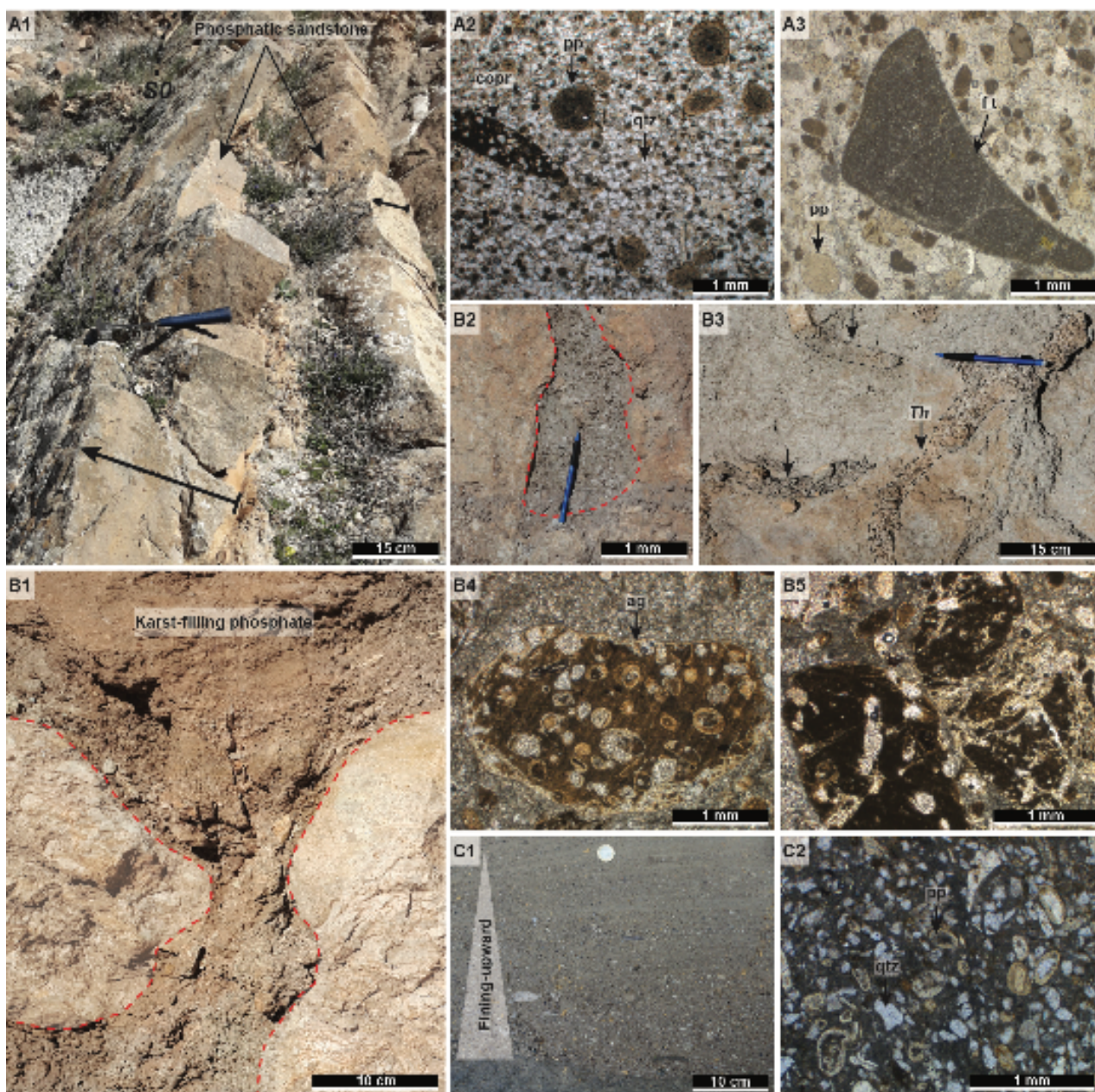
Fig. 8. Transported and reworked phosphate lithofacies (Allochthonous). (A1) Field photograph showing phosphatic sandstones. (A2-3) Transmitted light photomicrograph illustrating the petrographic composition of a phosphatic sandstone. (B1) Field photograph showing karst-filling phosphate. (B2) Granule-sized phosphate fill of karst. Dotted red line underlines the cavity. (B3) *Thalassinoides* burrows filled with granule-sized phosphate. (B4-5) Transmitted light photomicrograph of karst-filling facies. (C1) Field photograph exhibiting the normal grading features within the gravity-driven phosphate sediments. (C2) Transmitted light photomicrograph illustrating the

petrographic composition of turbiditic phosphate. **S0:** stratification plane; **pp:** peloid; **copr:** coprolite; **ft:** fish tooth; **ag:** agglomerated grains; **qtz:** quartz; **Th:** *Thalassinoides.*

8. Sequence stratigraphy

Sequence stratigraphy is used to visualize the organization of the phosphate-rich sediments and their position regarding the different stages of the relative sea-level variations (Fig. 9).The sequence stratigraphic framing, used in this study, is based on regional correlations of major key stratigraphic surfaces and facies changes. These regionally traceable surfaces reflect stratigraphic breaks and sedimentologic turnarounds, which thereby constitute reliable correlation datums. In this carbonate-dominated context, we adopted a transgressive-regressive sequence model (Embry, 1993, 1995; Embry and Johannessen, 1993) corresponding to sedimentary stacks embedded between two transgressive surfaces. These surfaces are used as sequence boundaries and then define depositional sequences. Two major stratigraphic datums have been identified (Fig. 9).

7.1. Major stratigraphic surfaces

The karstic surface (basal transgressive surface)

Located at the lower parts of the studied sections, this surface corresponds to the top of a karstic system affecting limestone and dolomite wackestones and packstones. The karst is developed as cm-wide interconnected dissolution fractures or as larger, m-scale cavities. The karstification process can act over 10 m depth. The karst infill varies from red silts to coarse-grained phosphate particles. The karstified lapiaz is filled and covered by transgressive sediments, including breccia and phospharudites. This karst system

formed in response to weathering processes when the carbonate layers were subaerially exposed due to sea-level fall. This extensively distributed key surface has been documented in the High Atlas areas as the D1 discontinuity, dated to the Upper Maastrichtian (Chellaï et al., 1995; Marzoqi et al., 1996; Marzoqi, 2001). It has also been recognized within the exploited basins of Gantour and Ouled Abdoun in central Morocco (Mouflih, 2015). It constitutes a sequence boundary and set as the lower datum for regional-scale correlations in this study.

The major maximum flooding surface/zone (MFS/MFZ)

Regionally, this surface bounds the outer platform carbonate sediments (FA5). In the northern margin of the Marrakesh High Atlas, this stratigraphic marker corresponds to a hardground surface, highlighted by massive accumulation of encrusting organisms, silicifications, iron-oxides crusts, and frequent bioturbation burrows filled with phosphate grains. Along the southern margin of the High Atlas, we defined maximum flooding zones (MFZ) relying on sedimentological criteria as the deepest facies within the whole vertical succession (Wilmsen, 2003). In the Ouarzazate basin, this maximum flooding zone is represented by nautiloids mudstones, while it consists of thin organic-rich layers in the Souss basin (Fig. 5K). This maximum flooding surface/zone is characterized by the low sedimentation rates and the scarcity of detrital particles. This typical stratigraphic marker reflects the transition from fining-upward to coarsening-upward cycle, highlighting the turnaround from transgressive to regressive phase. It is set as the upper datum for regional correlations.

Our nannoflora determinations (Fig. 3) indicate that the major MFS, which we correlate across the study area, is dated to the NP6 biozone i.e. at the transition between the Selandian and Thanetian, at around 59 Ma (Gradstein et al., 2012). The overlying

regressive hemicycle extends at least until the NP9 biozone (end-Thanetian). However, the top of this section is truncated by syntectonic Neogene alluvial fans, and it is likely that in other more complete sections, the regressive hemicycle lasts until the Eocene (Marzoqi, 2001). Consequently, our correlation across the studied area indicates that the interval between the karst surface and the major MFS is Danian-Selandian in age, assuming a Maastrichtian age for the formations affected by the karst (see review in Marzoqi, 2001).

7.2. Depositional sequence organization

The studied sedimentary succession was deposited during a relative sea-level cycle as defined by the major stratigraphic surfaces and facies evolution (Fig. 9). Higher-order sequences (third or fourth-order?) were identified below the major MFS (Fig. 9). These depositional sequences are bounded by minor stratigraphic surfaces and show facies shifts mirroring the relative sea-level changes. Four sequences were defined from the base to the top (Fig. 9):

<u>Sequence (S1)</u>

This sequence consists of carbonate material corresponding to the first recorded marine incursion within the studied series. S1 mantles the Senonian red continental sediments. S1 consists of dolomitic wackestones and packstones with bivalve dominance (Fig. 4J-L). It is bounded to the top by the major karstic surface and constitutes the regressive phase of a second-order transgressive/regressive cycle. It is very reduced or even absent within the eastern parts of the Ouarzazate basin. The upper parts of the sequence are probably absent due to karstification and erosion. No record of this sequence, interpreted of a Maastrichtian age (Marzoqi et al., 1996), was found around the Amizmiz area, where it is

considered as an erosional gap of the upper parts of the Maastrichtian (Chellaï et al., 1995).

Sequence (S2)

This sequence, coincides with the earliest recorded Cenozoic sediments(Chellaï et al., 1995; Marzoqi et al., 1996). It develops above the major karstic surface (Fig. 9). S2 varies in thickness from 10 m to up to 40 m. The transgressive part of the sequence begins with dolomudstone breccia and phospharudites. S2 evolves in a shallow-marine inner platform setting producing carbonates. Within the Ouarzazate basin, the MFS can be placed within wackestone to packstone carbonates, while it corresponds within the other regions to phosphatic hardgrounds. Within the Marrakesh High Atlas basin, this sequence exhibits the accumulations of phosphatic sandstones and the development of shoal bodies. The regressive part shows a distinct facies transition from shallow-water carbonates to thin continental red sediments and local karsts, emphasizing the shoreline seaward shifting. The presence of significant phosphate accumulations at the early transgressive parts of S2 is a distinctive feature of the sections from the Ouarzazate basin. To the north of the High Atlas, the phosphate accumulation corresponds to isolated phosphatic sandstones. This S2 sequence is lacking in the Amizmiz region, which suggests a probable paleogeographic high, preventing the deposition of this sequence.

Sequence (S3)

This sequence shows a similar transgressive-regressive evolution. The first transgressive sediments are represented by high-energy shallow-water carbonate facies, mainly calcarenites and coquina beds, being shallower eastwards, showing more terrigenous content (Fig. 4O-P). The MFS within the Marrakesh High Atlas and Souss basins,

44

corresponds to burrowed firm-grounds filled with phosphatic sediment, while it is represented by muddy carbonate sediments in the Ouarzazate basin. The regressive hemi-sequence marks an evolution from shoal and platform carbonates to continental red sediments, including red clay and silt. This interval is thicker in the easternmost part of the Ouarzazate basin.

Sequence (S4)

This sequence is the thickest in the whole succession, in every studied section (Fig. 9). It is characterized by lateral facies changes and significant phosphate accumulations. The transgressive system within S4 exhibits muddy carbonates and marls passing to packstone and grainstone carbonates with typical distal fauna, which characterizes a deepening upward trend with a facies transition from inner platform to outer platform, and finally to basin facies. The turnaround to the regressive part is marked by MFS, laterally changing to MFZ. In the northern border of the Marrakesh High Atlas, the MFS corresponds to a hardground surface showing echinoid accumulation (Fig. 5D), silicification, bioturbation, and phosphate grains on the hardground and filling the burrows. In the Souss basin, the MFZ corresponds to a thin layer (10 cm-thick) of organic-rich sediments while it is represented by nautiloids mudstone carbonate in the Ouarzazate basin (Fig. 5I). This correlative surface represents the most distal conditions within each measured section, in the whole studied area. The onset of the regressive system corresponds mostly to outer platform facies. Within the northern border of the Marrakesh High Atlas, these facies correspond to phosphatic marl intervals. These pristine phosphatic marls are restricted to this part of the sequence and are found only along the northern border of the High Atlas. Upwards, the regressive trend is marked by a progressive facies transition from marine carbonates to continental red beds, lacustrine

carbonate, paleosols horizons, and debris-flow conglomerate, respectively. Finally, Sequence 4 is truncated by Neogene molassic sediments derived from the erosion of the uprising High Atlas (Fig. 4B) (El Harfi et al., 2001; Görler et al., 1988).
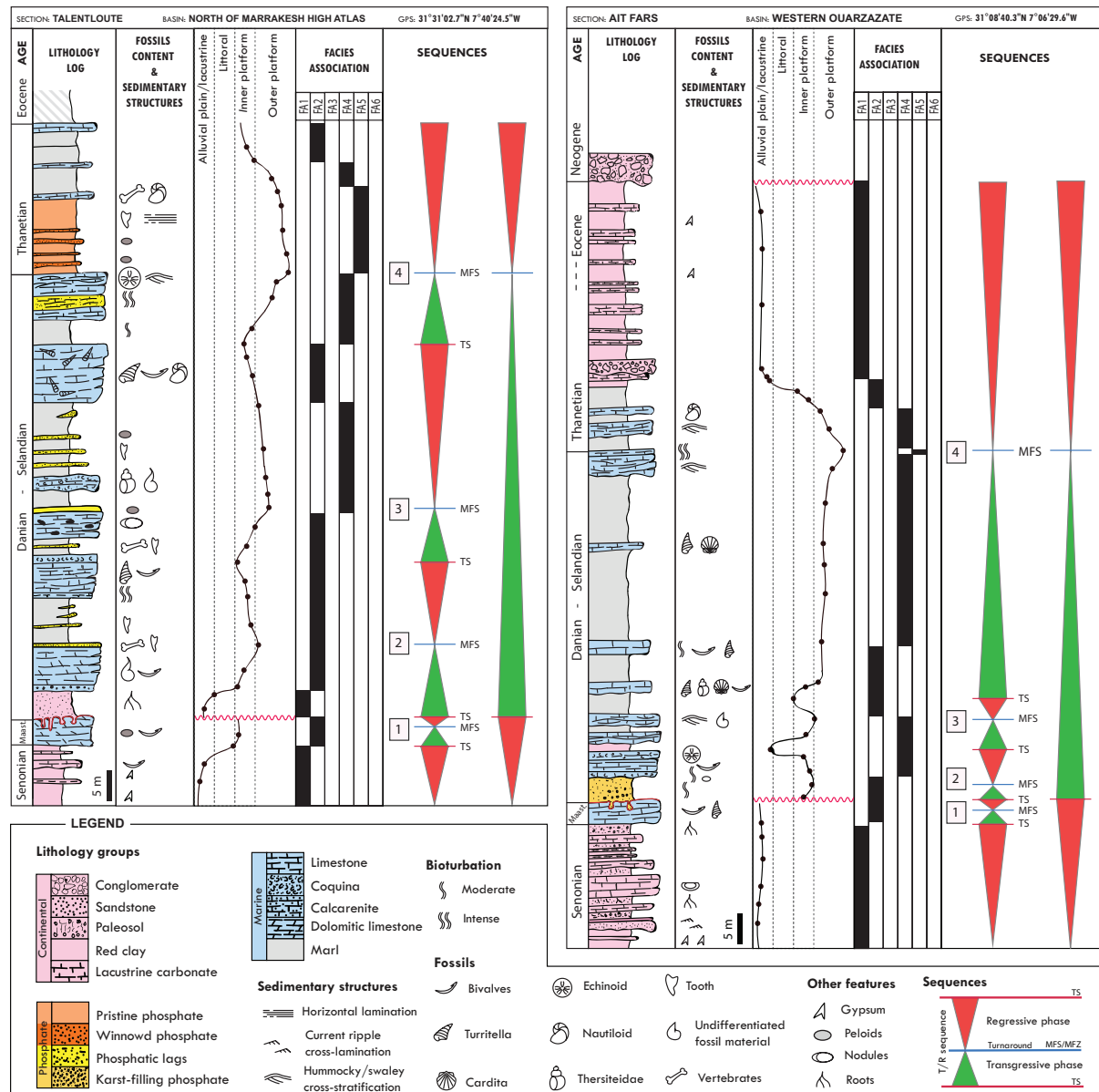

Fig. 9. Detailed logs (Talentloute and Ait Fars sections) showing the sedimentary evolution of the series and highlighting the sequence stratigraphic organization of the defined depositional sequences. The sequences are bounded by major and minor stratigraphic surfaces and are emphasized by facies shifts.

9. Discussion

The diversity of phosphate lithofacies within the Upper Cretaceous-Paleogene series of the High Atlas emphasizes the effects and interplay of different processes and controls over the phosphate sedimentation, within the studied marine platform system (Fig. 10). The fine laminated phosphatic marls deposited by settling suggest that pristine phosphate formed within the outer parts of the marine platform under low-energy conditions, below the storm wave-base. The formation of the primary phosphate grains (peloids) is believed to take place within closed and reduced pore water microsystems (Jarvis et al., 1994), in the unlithified sediment, which allows peloid growth up to mm-size diameter. Phosphorus is released to pore water from organic matter, Fe-oxyhydroxides, and clay minerals, mainly by microbial mediation (Jarvis et al., 1994; Krajewski et al., 1994; Hiatt et al., 2015; Pufahl and Groat, 2017), and then precipitates along with other chemical elements (F and Ca) as authigenic francolite. The latter corresponds to peloids scattered within a muddy matrix. Such primary phosphate sediment may undergo several sedimentary differentiation processes, leading to the formation of different phosphate lithofacies (Fig. 10). This differentiation is controlled by autocyclic and allocyclic processes. Firstly, autocyclic physical processes include hydrodynamic winnowing, reworking, and transporting. Storm and bottom currents sweep the pristine phosphate at the water-sediment interface to winnow the fine-grained material which is consequently removed, resuspended, laterally transported and redeposited away when the energy decreases. This hydrodynamic process causes the in-situ enrichment in phosphatic peloids, forming the so-called winnowed phosphate. When winnowing is repeated, it can lead to the formation of granular phosphate. This natural beneficiation process significantly enriches the phosphate grade and leads to economic

accumulations (Zhang et al., 2019). Transport and wave reworking of previously pristine and associated winnowed phosphate, produce phosphatic lags. This occurs in the proximal parts of the platform, at the vicinity of shoal complexes which act as morphologic traps for this phosphate lithofacies. Reworking eliminates the fine-grained portion of the sediments but integrates coarser detrital grains instead, including quartz, lithoclasts, and bone fragments, which counteracts the enrichment process of the phosphate grade. Gravity flows are responsible for the basinward redistribution of all previously described phosphate lithofacies. In the slope and basin, transported phosphates are redeposited with other terrigenous components in the form of turbiditic beds, showing normal grading patterns, and their association with thin black shales indicates deep depositional environment, below storm wave-base.
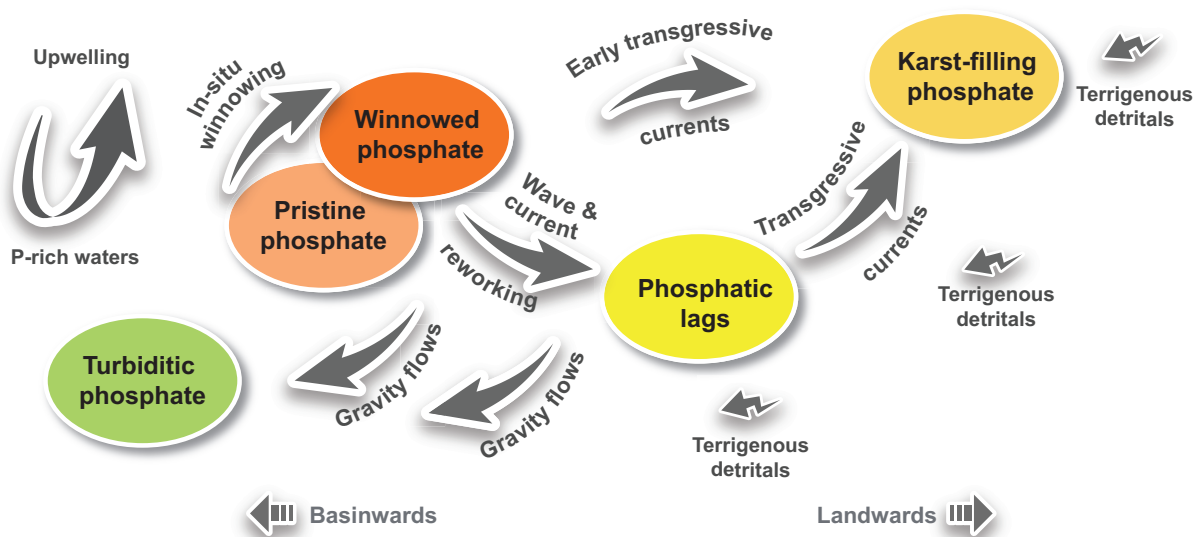
Fig. 10. Flow diagram showing the genetic links between the different types of phosphate identified in this study and highlighting the possible scenarios of sedimentary differentiation, as well as the sedimentary processes involved.

In addition to the aforementioned processes, the sedimentary differentiation of phosphate is further enhanced by allocyclic processes acting at the scale of the whole margin. Correspondingly, allocyclic (tectono-eustatic) relative sea-level variations generate correlative stratigraphic surfaces with which the main phosphate accumulation events are associated. Relative sea-level rise creates deepening upward sequences until reaching the maximum flooding surface (or zone). The pristine and associated winnowed phosphates are found preferentially above this surface (Fig. 11), which reflects relatively high bathymetric conditions, suitable for phosphogenesis (Föllmi, 1990). This pristine phosphate accumulation can be preserved in-situ or completely redistributed. Relative sea-level fall induces the fair-weather wave-base and storm wave-base to intercept the seafloor, which allows the previously deposited pristine phosphate to be reworked and transported. Accordingly, phosphatic lags are found in the regressive interval of the sequences (Fig. 11). Relative sea-level fall also causes the subaerial exposure of the proximal inner shelf, with the development of widespread karstification of carbonates. During subsequent sea-level rise, early transgressive landwards currents, erode, rework, and transport sediments accumulated on the inner shelf (Cattaneo and Steel, 2003). In the study area, karst-filling phosphates, showing evidence of landward transport and redeposition from older phosphate accumulations (agglomerated and fragmented phosphate grains) indicate that phosphatic lags and/or granular phosphate previously accumulated on the shelf have been redeposited within and above the karstic pockets. Moreover, the deposition of such phosphate grains above a subaerial karst surface is an evidence for its allochthonous character.

Fig. 11. Fence diagram showing the lateral correlation of the studied sections in the High Atlas. The major MFS is set as the reference datum for horizontalization. The lateral and vertical distribution of the different phosphate types is highlighted with respect to the different stages of the sea-level variations.

The sedimentary record of the High Atlas phosphate series reflects the interaction of allocyclic controls and autocyclic processes through lateral shifts induced by relative sea-level variations. Hence, the spatial distribution of the different phosphate types is eustatically and paleogeographically controlled. Our results indicate that the late Cretaceous-Paleogene series of the High Atlas were deposited in a single shallow platform passing to basin deepening northwestward, which is consistent with the views of Herbig and Trappe, (1994). During the studied interval, central Morocco was flooded over a wide area reaching the emerged Anti-Atlas (Herbig and Trappe, 1994). At that time, the Atlantic margin was characterized by an active upwelling system (Holbourn et al., 1999) bringing in deeper P-rich waters (Lucas and Prévôt, 1975) to the platform margin, where the primary phosphogenesis was stimulated in the phosphogenic window (Trappe, 1998).

At the end of the Maastrichtian, a general regression caused the subaerial exposure of the whole Atlasic basin resulting in a westward shift of the phosphogenic window, the creation of extensive karstification, and development paleosol horizons. As relative sea-level rose again during the Danian and Selandian (Fig. 12A), the phosphate previously formed in the margin and reworked on the shelf were transported landward by early transgressive currents, and trapped within karst pockets in the Ouarzazate basin. In the same time, phosphogenesis was still active in the phosphogenic window and hydrodynamics was reworking phosphate sediments in the inner platform,

corresponding to the present-day Marrakesh High Atlas, where phosphatic lags are found.

Relative sea-level rise during the Selandian progressively moved the phosphogenic window towards the southeast. During the Selandian-Thanetian transition (Fig. 12B), the maximum bathymetry was reached and the phosphogenic window was active within the outer platform (Marrakesh High Atlas basin). Interbedded pristine and winnowed phosphates were formed, preserved, and buried under subsequent carbonate and marl sequences. Storm and wave currents episodically reworked part of the winnowed phosphate and transported it landward up to the Ouarzazate basin, where only few phosphatic lags are described. The absence of pristine and associated winnowed phosphate within the Ouarzazate basin implies that paleoenvironments in this part of the system were never deep enough to form and preserve this facies. During this time, the Souss basin presented relatively deep environments where offshore organic-rich sediments and turbiditic phosphate beds were preserved. During the late Cretaceous-Paleogene interval, the detrital inputs were more expressed within the east of the Ouarzazate basin (close to the Anti-Atlas terrigenous sources) and Souss basin (gravity flows, maybe connected to a deltaic system), while only minor amounts of coarse clastic sediments were delivered to the Marrakesh High Atlas basin. Such small detrital input contributed to the observed low sedimentation rate in this part of the basin. This sediment starvation is important for the productivity of the phosphate factory as it drastically reduces the dilution of the phosphatic particles within the ambient sedimentation (Filippelli, 1997).
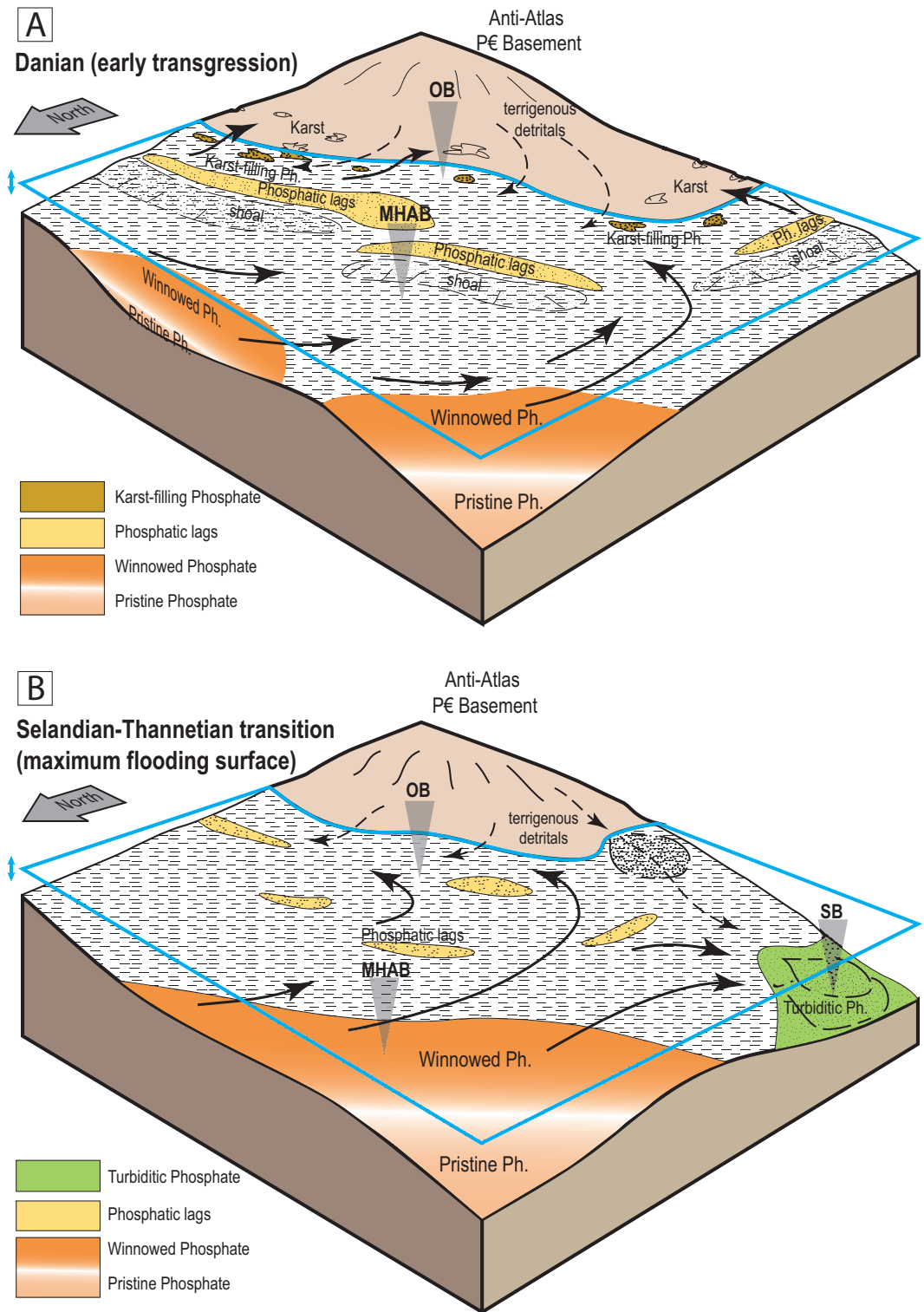
Fig. 12. 3D paleogeographic model for the accumulation of phosphate within the High Atlas of Morocco illustrating the different accumulation modes of phosphate and highlighting the shifting of the primary phosphogenesis window in two successive periods of the evolution of the studied series. OB: Ouarzazate basin; MHAB: Marrakesh High Atlas basin; SB: Souss basin.

10. Conclusions

Our study of the phosphate sequences of the Moroccan High Atlas brings new understanding on the sedimentological controls on their accumulation and preservation in the Maastrichtian to Paleocene sedimentary record. In particular, the markedly varying types of phosphate sediments, and the diversity of sedimentary environments where they were found, do not result from different phosphogenesis processes in a range of paleoenvironmental settings. Lithofacies analyses, combined with basin-scale correlations allowed to identify the genetic links between five type of phosphate-rich-sediments. Primary phosphogenesis leads to the formation of pristine phosphate, in the phosphogenesis window, offshore of a carbonate platform, and under the control of upwelling currents. All other types of phosphate-rich sediments, known as reworked phosphates (Glenn et al., 1994; Pufahl and Groat, 2017), derive from sedimentary differentiation of this authigenically-formed pristine phosphate. On one hand, the sedimentary differentiation is controlled by the interaction of hydrodynamic autocyclic processes, such as wave and storm winnowing, currents across the platform, as shown by the spatial distribution of the five types of phosphate across the basin. On the other hand, tectono-eustatic allocyclic forcing modifies the position of the phosphogenesis window, in response to relative sea-level variations. As a result, the whole phosphogenic system is shifting landward or basinward during relative sea-level rise and fall, respectively. The main phosphate interval in the Marrakesh High Atlas corresponds to alternations of pristine and granular phosphates, that accumulated and were preserved above a major maximum flooding surface, which we date to the lower Thanetian.

54

On a global scale, we show that upwelling-controlled, primary phosphogenesis, allows the formation of pristine phosphate, which typically results in low-grade phosphatic sediments, as phosphate grains are scattered within the host marls. The phosphate enrichment, leading to economic-grade ore, requires hydrodynamic processes. Repeated storm and currents winnowing is an effective enrichment mode of the phosphate ore grade. Winnowed granular phosphate accumulations represent the richest phosphate type, which is accumulated on the outer platforms, close to the storm wave-base, away from the main terrigenous sources, and which is preserved during the early regressive hemi-sequence. These new insights on the controlling parameters of phosphate accumulation will help the exploration and exploitation of this non-renewable resource.

Acknowledgments

References

Abed, A.M., Sadaqah, R., Al-Jazi, M., 2007. Sequence stratigraphy and evolution of Eshidiyya phosphorite platform, southern Jordan. Sediment. Geol. 198, 209–219. https://doi.org/10.1016/J.SEDGEO.2006.12.008

Agnini, C., Fornaciari, E., Raffi, I., Rio, D., Röhl, U., Westerhold, T., 2007. High-resolution nannofossil biochronology of middle Paleocene to early Eocene at ODP Site 1262: Implications for calcareous nannoplankton evolution. Mar. Micropaleontol. 64, 215–248. https://doi.org/10.1016/j.marmicro.2007.05.003

Algouti, Ah, Algouti, Ab, Taj-Eddine, K., 1999. Le Sénonien du Haut Atlas occidental, Maroc: sédimentologie, analyse séquentielle et paléogéographie. J. African Earth Sci. 29, 643–658. https://doi.org/10.1016/S0899-5362(99)00121-9

Arambourg, C., 1952. Les vertébrés fossiles des gisements de phosphates (Maroc-Algerie-Tunisie). Notes Mem. du Serv. Geol. du Maroc 92, 1–372.

Arambourg, C., 1937. Nouvelles observations sur la série phosphatée du Maroc. Comptes rendus sommaires des séances la Société Géologique Fr. 7, 183–184.

Bachmann, M., Hirsch, F., 2006. Lower Cretaceous carbonate platform of the eastern Levant (Galilee and the Golan Heights): stratigraphy and second-order sea-level change. Cretac. Res. 27, 487–512.

Baioumy, H.M., Tada, R., Gharaie, M.H.M., 2007. Geochemistry of Late Cretaceous phosphorites in Egypt: Implication for their genesis and diagenesis. J. African Earth Sci. 49, 12–28. https://doi.org/10.1016/J.JAFREARSCI.2007.05.003

Bardet, N., Gheerbrant, E., Noubhani, A., Cappetta, H., Jouve, S., Bourdon, E., Suberbiola, X.P., Jalil, N.-E., Vincent, P., Houssaye, A., 2017. Les Vertébrés des phosphates crétacés-paléogènes (72, 1-47, 8 Ma) du Maroc, in: Mémoires de la Société Géologique de France. Soc. Géol. de France, pp. 351–452.

Baturin, G.N., 1982. Phosphorite on the sea floor: origin, composition and distribution, in: Developments in Sedimentology. Elsevier, p. 355.

Beauchamp, W., Allmendinger, R.W., Barazangi, M., Demnati, A., El Alji, M., Dahmani, M., 1999. Inversion tectonics and the evolution of the High Atlas Mountains, Morocco, based on a geological-geophysical transect. Tectonics 18, 163–184. https://doi.org/10.1029/1998TC900015

Belfkira, O., 1980. Evolutions sédimentologiques et géochimiques de la série phosphatée du Maestrichtien des Ouled Abdoun (Maroc). Université Scientifique et Médicale de Grenoble, France.

Blair, T.C., McPhe, J.G., 1994. Alluvial Fans and their Natural Distinction from Rivers Based on Morphology, Hydraulic Processes, Sedimentary Processes, and Facies Assemblages. SEPM J. Sediment. Res. Vol. 64A, 450–489. https://doi.org/10.1306/D4267DDE-2B26-11D7-8648000102C1865D

Boujo, A., 1976. Contribution à l'étude géologique du gisement de phosphate crétacé-éocène des Ganntour (Maroc occidental). Sci. Géologiques, Bull. mémoires 43, 227.

Bown, P. R., Young, J. R. , 1997. Proposals for a revised classification system for calcareous nannoplankton. Journal of Nannoplankton Research, 19(1), 15-47.

Bramlette, M. N., Martini, E., 1964. The great change in calcareous nannoplankton fossils between the Maestrichtian and Danian. Micropaleontology, 291-322.

Bramlette, M. N., Riedel, W. R., 1954. Stratigraphic value of discoasters and some other microfossils related to Recent coccolithophores. Journal of Paleontology, 28, 385-403.

Brives, A., 1905. Les terrains crétacés dans le Maroc occidental. Bull. Soc. Géol. Fr. 5, 905.

Burnett, J.A., 1998. UpperCretaceous. In: Bown, P.R. (Ed.) Calcareous Nannofossil Biostratigraphy. British Micropalaeontological Society Publication Series, Chapman & Hall, pp. 132-199.

Burchette, T.P., Wright, V.P., 1992. Carbonate ramp depositional systems. Sediment. Geol. 79, 3–57.

Cappetta, H., 1993. Sélaciens nouveaux (Chondrichthyes, Neoselachii) du Paléocène supérieur de la région d'Ouarzazate, Maroc. Paläontologische Zeitschrift 67, 109–122. https://doi.org/10.1007/BF02985873

Cappetta, H., 1986. Un nouveau genre de selacien (batomorphii, myliobatiformes) de l'Ypresien des ouled abdoun, Maroc. Geobios 19, 635–640.

Cappetta, H., 1981. Additions a la faune de sélaciens fossilesdu Maroc. 1: Sur la présence des genres Heptranchias, Alopias etOdontorhytis dans l'Yprésien des Ouled Abdoun. Geobios 14, 563–575. https://doi.org/10.1016/S0016-6995(81)80137-4

Cappetta, H., Bardet, N., Pereda Suberbiola, X., Adnet, S., Akkrim, D., Amalik, M., Benabdallah, A., 2014. Marine vertebrate faunas from the Maastrichtian phosphates

of Benguerir (Ganntour Basin, Morocco): Biostratigraphy, palaeobiogeography and palaeoecology. Palaeogeogr. Palaeoclimatol. Palaeoecol. 409, 217–238. https://doi.org/10.1016/j.palaeo.2014.04.020

Cappetta, H., Jaeger, J.J., Sabatier, B., Sigé, B., Sudre, J., Vianey-Liaud, M., 1987. Compléments et précisions biostratigraphiques sur la faune paléocène à Mammifères et Sélaciens du bassin d'Ouarzazate (Maroc). Tert. Res. 8, 147–157.

Cattaneo, A., Steel, R.J., 2003. Transgressive deposits: A review of their variability. Earth-Science Rev. 62, 187–228. https://doi.org/10.1016/S0012-8252(02)00134-4

Cheel, R.J., Leckie, D.A., 1993. Hummocky cross-stratification. Sedimentol. Rev. 1, 103–122.

Chellaï, E.H., Marzoqi, M., Pascal, A., Mouflih, M., 1995. Stratigraphy and evolution of Upper Cretaceous-Palaeogene sedimentary systems in the Marrakesh High Atlas (Morocco). C.R. Acad. Sci. Paris Série II a, 745–752.

Chellai, E.H., Perriaux, J., 1996. Evolution geodynamique d'un bassin d'avant-pays du domaine atlasique (Maroc): exemple des dépôts néogènes et quaternaires du versant septentrional de l'Atlas de Marrakech. Comptes rendus l'Académie des Sci. Série 2. Sci. la terre des planètes 322, 727–734.

Diaz, J., Ingall, E., Benitez-Nelson, C., Paterson, D., Jonge, M.D. de, McNulty, I., Brandes, J.A., 2008. Redox Stabilization of the Atmosphere and Oceans by Phosphorus-Limited Marine Productivity. Science, 271(5248), 493–496. https://doi.org/10.1126/science.271.5248.493

Dott Jr, R.H., 1974. Cambrian tropical storm waves in Wisconsin. Geology 2, 243–246.

Dott, R.H., Bourgeois, J., 1982. Hummocky stratification: Significance of its variable bedding sequences. GSA Bull. 93, 663–680. https://doi.org/10.1130/0016-7606(1982)93<663:hssoiv>2.0.co;2

Ekdale, A.A., Bromley, R.G., 2003. Paleoethologic interpretation of complex Thalassinoides in shallow-marine limestones, Lower Ordovician, southern Sweden. Palaeogeogr. Palaeoclimatol. Palaeoecol. 192, 221–227.

Ekdale, A.A., Bromley, R.G., 1984. Comparative Ichnology of Shelf-Sea and Deep-Sea Chalk. J. Paleontol. 58, 322–332.

El Harfi, A., Lang, J., Salomon, J., Chellai, E.H., 2001. Cenozoic sedimentary dynamics of the ouarzazate foreland basin (Central High Atlas Mountains, Morocco). Int. J. Earth Sci. 90, 393–411. https://doi.org/10.1007/s005310000115

Ellouz, N., Patriat, M., Gaulier, J.M., Bouatmani, R., Sabounji, S., 2003. From rifting to Alpine inversion: Mesozoic and Cenozoic subsidence history of some Moroccan basins. Sediment. Geol. 156, 185–212. https://doi.org/10.1016/S0037-0738(02)00288-9

Embry, A.F., 1995. Sequence boundaries and sequence hierarchies: Problems and proposals. Nor. Pet. Soc. Spec. Publ. 5, 1–11. https://doi.org/10.1016/S0928-8937(06)80059-7

Embry, A.F., 1993. Transgressive-regressive (T-R) sequence analysis of the Jurassic succession of the Sverdrup Basin, Canadian Arctic Archipelago. Can. J. Earth Sci. 30, 301–320. https://doi.org/10.1139/e93-024

Embry, A.F., Johannessen, E.P., 1993. T–R sequence stratigraphy, facies analysis and reservoir distribution in the uppermost Triassic–Lower Jurassic succession, western Sverdrup Basin, Arctic Canada, in: Norwegian Petroleum Society Special Publications. Elsevier, pp. 121–146. https://doi.org/10.1016/B978-0-444-88943-0.50013-7

Fekkak, A., Ouanaimi, H., Michard, A., Soulaimani, A., Ettachfini, E.M., Berrada, I., El Arabi, H., Lagnaoui, A., Saddiqi, O., 2018. Thick-skinned tectonics in a Late Cretaceous-Neogene intracontinental belt (High Atlas Mountains, Morocco): The flat-ramp fault control on basement shortening and cover folding. J. African Earth Sci. 140, 169–188. https://doi.org/10.1016/j.jafrearsci.2018.01.008

Fick, C., Toldo, E.E., Puhl, E., 2018. Shell concentration dynamics driven by wave motion in flume experiments: Insights for coquina facies from lake-margin settings. Sediment. Geol. 374, 98–114. https://doi.org/10.1016/J.SEDGEO.2018.08.002

Filippelli, G.M., 2011. Phosphate rock formation and marine phosphorus geochemistry: The deep time perspective. Chemosphere 84, 759–766. https://doi.org/10.1016/j.chemosphere.2011.02.019

Filippelli, G.M., 1997. Controls on phosphorus concentration and accumulation in oceanic sediments. Mar. Geol. 139, 231–240. https://doi.org/10.1016/S0025-3227(96)00113-2

Flügel, E., 2010. Microfacies of Carbonate Rocks: Analysis, Interpretation and Application, Second edi. ed. Springer Heidelberg Dordrecht London New York. https://doi.org/DOI 10.1007/10.1007/978-3-642-03796-2

Föllmi, K.B., 1996. The phosphorus cycle, phosphogenesis and marine phosphate-rich deposits. Earth-Science Rev. 40, 55–124. https://doi.org/10.1016/0012-8252(95)00049-6

Föllmi, K.B., 1990. Condensation and phosphogenesis: example of the Helvetic mid-Cretaceous (northern Tethyan margin). Geol. Soc. London, Spec. Publ. 52, 237–252. https://doi.org/10.1144/GSL.SP.1990.052.01.17

Föllmi, K.B., Garrison, R.E., Ramirez, P.C., Zambrano-Ortiz, F., Kennedy, W.J., Lehner, B.L., 1992. Cyclic phosphate-rich successions in the upper Cretaceous of Colombia. Palaeogeogr. Palaeoclimatol. Palaeoecol. 93, 151–182. https://doi.org/10.1016/0031-0182(92)90095-M

Föllmi, K.B., Hofmann, H., Chiaradia, M., de Kaenel, E., Frijia, G., Parente, M., 2015. Miocene phosphate-rich sediments in Salento (southern Italy). Sediment. Geol. 327, 55–71. https://doi.org/10.1016/j.sedgeo.2015.07.009

Föllmi, K.B., Weissert, H., Lini, A., 1993. Nonlinearities in Phosphogenesis and Phosphorus-Carbon Coupling and Their Implications for Global Change, in: Interactions of C, N, P and S Biogeochemical Cycles and Global Change. Springer Berlin Heidelberg, pp. 447–474. https://doi.org/10.1007/978-3-642-76064-8_18

Frey, R.C., 1987. The Paleoecology of a Late Ordovician Shale Unit from Southwest Ohio and Southeastern Indiana. J. Paleontol. 61, 242–267.

Freytet, P., Plaziat, J.-C., 1982. Continental Carbonate Sedimentation and Pedogenesis - Late Cretaceous and Early Tertiary of Southern France. Schweizerbart Science Publishers, Stuttgart, Germany.

Freytet, P., Verrecchia, E., 1989. Les carbonates continentaux du pourtour méditerranéen: microfaciès et milieux de formation. Méditerranée 68, 5–28.

Frizon De Lamotte, D., Fourdan, B., Leleu, S., Leparmentier, F., De Clarens, P., 2015. Style of rifting and the stages of Pangea breakup. Tectonics. https://doi.org/10.1002/2014TC003760

Frizon de Lamotte, D., Leturmy, P., Missenard, Y., Khomsi, S., Ruiz, G., Saddiqi, O., Guillocheau, F., Michard, A., 2009. Mesozoic and Cenozoic vertical movements in the Atlas system (Algeria, Morocco, Tunisia): An overview. Tectonophysics 475, 9–28. https://doi.org/10.1016/j.tecto.2008.10.024

Fürsich, F., Oschmann, W., 1993. Shell beds as tools in basin analysis: The Jurassic of Kachchh, western India. J. Geol. Soc. London. 150, 169–185. https://doi.org/10.1144/gsjgs.150.1.0169

Galli-Olivier, C., Garduno, G., Gamino, J., 1990. Phosphorite deposits in the Upper Oligocene, San Gregorio Formation at San Juan de la Costa, Baja California Sur, Mexico, in: Phosphate Deposits of the World, Vol. 3. Neogene to Modern Phosphorites. Cambridge University Press, pp. 122–126.

Gauthier, H., 1960. Contribution à l'étude géologique des formations post-liasiques des bassins du Dadès et du Haut Todra (Maroc méridional). Notes Mem. du Serv. Geol. du Maroc 119, 212.

Gheerbrant, E., Cappetta, H., Feist, M., Jaeger, J.-J., Sudre, J.V.-L., Sigé, B., 1993. Succession of faunas of vertebrates from the Upper Paleocene and the Early Eocene in the Ouarzazate basin (Morocco). Geological context, biostratigraphical and

paleogeographical scope. Newsletters Stratigr. 28, 33–58. https://doi.org/10.1127/nos/28/1993/33

Gheerbrant, E., Sudre, J., Sen, S., Abrial, C., Marandat, B., Sigé, B., Vianey-Liaud, M., 1998. Nouvelles données sur les mammifères du Thanétien et de l'Yprésien du bassin d'Ouarzazate (Maroc) et leur contexte stratigraphique. Palaeovertebrata 27, 155–202.

Glenn, C.R., Föllmi, K.B., Riggs, S.R., Baturin, G.N., Grimm, K.A., Trappe, J., Abed, A.M., Galli-Olivier, C., Garrison, R.E., Ilyin, A. V., Jehl, C., Rohrlich, V., Sadaqah, R.M.Y., Schidlowski, M., Sheldon, R.E., Seigmund, H., 1994. Phosphorus and phosphorites: sedimentology and environments of formation. Eclogae Geol. Helv. 87, 747–788. https://doi.org/10.5169/seals-167476

Glennie, K.W., 1970. Desert Sedimentary Environments, in: Developments in Sedimentology. Elsevier, Amsterdam, p. 222. https://doi.org/10.1017/CBO9781107415324.004

Görler, K., Helmdach, F.-F., Gaemers, P., Heißig, K., Hinsch, W., Mädler, K., Schwarzhans, W., Zucht, M., 1988. The uplift of the central High Atlas as deduced from neogene continental sediments of the Ouarzazate province, Morocco, in: Jacobshagen, V.H. (Ed.), The Atlas System of Morocco: Studies on Its Geodynamic Evolution. Springer Berlin Heidelberg, Berlin, Heidelberg, pp. 359–404. https://doi.org/10.1007/BFb0011601

Gradstein, F.M., Ogg, J.G., Schmitz, M., Ogg, G., 2012. The geologic time scale 2012. elsevier.

Hafid, M., Zizi, M., Bally, A.W., Ait Salem, A., 2006. Structural styles of the western onshore

and offshore termination of the High Atlas, Morocco. Comptes Rendus - Geosci. 338, 50–64. https://doi.org/10.1016/j.crte.2005.10.007

Hay, W. W., Mohler, H. P., Roth, P. H., Schmidt, R. R., Boudreaux, J. E., 1967. Calcareous Nannoplankton Zonation of the Cenozoic of the Gulf Coast and Caribbean-Antillean Area, and Transoceanic Correlation. Trans. Gulf Coast Assoc. Geol. Soc. 17, 428-480.

Herbig, H.-G., Trappe, J., 1994. Stratigraphy of the Subatlas Group (Maastrichtian - Middle Eocene, Morocco). Newsletters Stratigr. 30, 125–165. https://doi.org/10.1127/nos/30/1994/125

Hiatt, E.E., Pufahl, P.K., Edwards, C.T., 2015. Sedimentary phosphate and associated fossil bacteria in a Paleoproterozoic tidal flat in the 1.85Ga Michigamme Formation, Michigan, USA. Sediment. Geol. https://doi.org/10.1016/j.sedgeo.2015.01.006

Holbourn, A., Kuhnt, W., El Albani, A., Pletsch, T., Luderer, F., Wagner, T., 1999. Upper Cretaceous palaeoenvironments and benthonic foraminiferal assemblages of potential source rocks from the western African margin, Central Atlantic. Geol. Soc. Spec. Publ. 153, 195–222. https://doi.org/10.1144/GSL.SP.1999.153.01.13

Hunter, R.E., 1977. Basic types of stratification in small eolian dunes. Sedimentology 24, 361–387. https://doi.org/10.1111/j.1365-3091.1977.tb00128.x

Jahnert, R., de Paula, O., Collins, L., Strobach, E., Pevzner, R., 2012. Evolution of a coquina barrier in Shark Bay, Australia by GPR imaging: Architecture of a Holocene reservoir analog. Sediment. Geol. 281, 59–74. https://doi.org/10.1016/J.SEDGEO.2012.08.009

Jarvis, I., Burnett, W.C., Nathan, Y., Almbaydin, F.S.M., Attia, A.K.M., Castro, L.N., Flicoteaux, R., Hilmy, M.E., Husain, V., Qutawnah, A.A., Serjani, A., Zanin, Y.N., 1994. Phosphorite Geochemistry - State-of-the-Art and Environmental Concerns. Eclogae Geol. Helv. 87, 643–700. https://doi.org/10.5169/seals-167474

Jasinski, S.M., 2018. Mineral commodity summaries: Phosphate Rock 122–123.

Kechiched, R., Laouar, R., Bruguier, O., Salmi-Laouar, S., Kocsis, L., Bosch, D., Foufou, A., Ameur-Zaimeche, O., Larit, H., 2018. Glauconite-bearing sedimentary phosphorites from the Tébessa region (eastern Algeria): Evidence of REE enrichment and geochemical constraints on their origin. J. African Earth Sci. 145, 190–200. https://doi.org/10.1016/j.jafrearsci.2018.05.018

Kidwell, S.M., 1986. Models for fossil concentrations: paleobiologic implications. Paleobiology 12, 6–24. https://doi.org/10.1017/S0094837300002943

Kocurek, G., 1991. Interpretation of Ancient Eolian Sand Dunes. Annu. Rev. Earth Planet. Sci. 19, 43–75. https://doi.org/10.1146/annurev.ea.19.050191.000355

Krajewski, K.P., Cappellen, P. van, Trichet, J., Kuhn, O., Lucas, J., Martín-Algarra, A., Prevot-Lucas, L., Tewari, V.C., Gaspar, L., Knight, R.I., Lamboy, M., 1994. Biological processes and apatite formation in sedimentary environments. Eclogae Geol. Helv. 87, 701–746.

Krinsley, D., Trusty, P., 1985. Environmental Interpretation of Quartz Grain Surface Textures, in: Zuffa, G.G. (Ed.), Provenance of Arenites. Springer Netherlands, Dordrecht, pp. 213–229. https://doi.org/10.1007/978-94-017-2809-6_10

Leprêtre, R., Missenard, Y., Saint-bezar, B., Barbarand, J., Delpech, G., Yans, J., Dekoninck, A., Saddiqi, O., 2015. Journal of African Earth Sciences The three main steps of the Marrakech High Atlas building in Morocco : Structural evidences from the southern foreland , Imini area. J. African Earth Sci. 109, 177–194. https://doi.org/10.1016/j.jafrearsci.2015.05.013

Lucas, J., Prévôt, L., 1975. Les marges continentales pieges geochimiques; l'exemple de la marge atlantique de l'Afrique a la limite Cretace-Tertiaire. Bull. la Soc. Geol. Fr. S7-XVII, 496–501. https://doi.org/10.2113/gssgfbull.s7-xvii.4.496

Major, J.J., 2003. Debris flow, in: Middleton, G. V. (Ed.), Encyclopaedia of Sediments and Sedimentary Rocks. Springer Netherlands, Dordrecht, pp. 186–188. https://doi.org/10.1007/978-1-4020-3609-5_58

Martini, E., 1971. Standard Tertiary and Quaternary calcareous nannoplankton zonation. Proc. II Planktonic Conf. Roma 1970, Roma, Tecnoscienza 2, 739–785.

Marzoqi, M., 2001. Les systèmes sédimentaires marins du Crétacé Terminal-Paleogene dans l'Atlas de Marrakech et le bassin de Ouarzazate. These d'état, Univ. Cadi Ayyad, Marrakech.

Marzoqi, M., Pascal, A., 2000. Séquences de dépôts et tectono-eustatisme à la limite Crétacé/Tertiaire sur la marge sud-téthysienne (Atlas de Marrakech et bassin de Ouarzazate, Maroc). Newsletters Stratigr. 38, 57–80. https://doi.org/10.1127/nos/38/2000/57

Marzoqi, M., Pascal, A., Chellai, E.H., Lang, J., 1996. Les séquences de depôts sur la rampe carbonatée maastrichtienne-paléogène en bordure nord orientale du Golfe

Atlantique dans la région d'Aït-Ourir (Atlas de Marrakech, Maroc). Bull. des Centres Rech. Explor. Elf-Aquitaine. Mémoire 511–520.

Mattauer, M., Tapponnier, P., Proust, F., 1977. Sur les mecanismes de formation des chaines intracontinentales; l'exemple des chaines atlasiques du Maroc. Bull. la Soc. Geol. Fr. S7-XIX, 521–526. https://doi.org/10.2113/gssgfbull.s7-xix.3.521

Miall, A.D., 1996. The Geology of Fluvial Deposits, 1st ed. Springer Berlin Heidelberg, Berlin, Heidelberg. https://doi.org/10.1007/978-3-662-03237-4

Michard, A., Saddiqi, O., Chalouan, A., de Lamotte, D.F., 2008. Continental Evolution : The Geology of Morocco, 1st ed. Springer.

Missenard, Y., Saddiqi, O., Barbarand, J., Leturmy, P., Ruiz, G., El Haimer, F.Z., de Lamotte, D.F., 2008. Cenozoic denudation in the Marrakech High Atlas, Morocco: Insight from apatite fission-track thermochronology. Terra Nov. 20, 221–228. https://doi.org/10.1111/j.1365-3121.2008.00810.x

Mohr, B., Fechner, G., 1986. Eine eozäne Mikroflora (Sporomorphae und Dinoflagellaten-Zysten) aus der Südatlas-Randzone westlich Boumalne du Dadès (Marokko). Berliner Geowissenschaftliche Abhandlungen,(A) 66, 381–414.

Moret, L., 1938. Contribution à la paléontologie des couches crétacées et éocènes du versant sud de l'Atlas de Marrakech. Notes Mem. du Serv. Geol. du Maroc 49, 104 p.

Mouflih, M., 2015. Les phosphates du Maroc central et du Moyen Atlas (Maastrichtien-Lutétien, Maroc): Sédimentologie, stratigraphie séquentielle, contexte génétique et valorisation. Doctorat d'Etat Es-sciences. Université Cadi Ayyad.

Murphy, D.H., Wilkinson, B.H., 1980. Carbonate deposition and facies distribution in a central Michigan marl lake. Sedimentology 27, 123–135. https://doi.org/10.1111/j.1365-3091.1980.tb01164.x

Nemec, W., Steel, R.J., 1984. Alluvial and coastal conglomerates : Their significant features and some comments on gravelly mass flow deposits. Sedimentol. gravels conglomerates Memoir 10, 1–31.

Notholt, A.J.G., 1985. Phosphorite resources in the Mediterranean (Tethyan) phosphogenic province : a progress report. Sci. Géologiques, Bull. mémoires 77, 9–17.

Noubhani, A., 2010. The selachians' faunas of the Moroccan phosphate deposits and the KT mass-extinctions. Hist. Biol. 22, 71–77. https://doi.org/10.1080/08912961003707349

Noubhani, A., Cappetta, H., 1994. Révision des Rhombodontidae (Neoselachii, Batomorphii) des bassins à phosphate du Maroc. Palaeovertebrata 23, 1–49.

Ollivier-Pierre, M.-F., 1982. La microflore du Paléocène et de l'Eocène des séries phosphatées des Ganntour (Maroc). Sci. Géologiques. Bull. 35, 117–127. https://doi.org/10.3406/sgeol.1982.1615

Ounis, A., Kocsis, L., Chaabani, F., Pfeifer, H.R., 2008. Rare earth elements and stable isotope geochemistry ($\delta 13C$ and $\delta 18O$) of phosphorite deposits in the Gafsa Basin, Tunisia. Palaeogeogr. Palaeoclimatol. Palaeoecol. 268, 1–18. https://doi.org/10.1016/j.palaeo.2008.07.005

Perch-Nielsen, K., 1985. Mesozoic calcareous nannofossils. In: Bolli, H.M., Saunders, J.B., Perch-Nielsen, K. (Eds.), Plankton Stratigraphy. Cambridge University Press, Cambridge, pp. 329–426.

Pickering, K., Stow, D., Watson, M., Hiscott, R., 1986. Deep-water facies, processes and models: a review and classification scheme for modern and ancient sediments. Earth Sci. Rev. 23, 75–174. https://doi.org/10.1016/0012-8252(86)90001-2

Platt, N.H., Wright, V.P., 1991. Lacustrine Carbonates: Facies Models, Facies Distributions and Hydrocarbon Aspects, in: Lacustrine Facies Analysis. John Wiley & Sons, Ltd, pp. 57–74. https://doi.org/10.1002/9781444303919.ch3

Posamentier, H.W., Walker, R.G., 2006. Facies models revisited. SEPM Special Publication 84 SEPM, Tulsa, Oklahoma.

Prévôt, L., 1988. Geochimie et petrographie de la formation a phosphate des ganntour (maroc): utilisation pour une explication de la genese des phosphorites cretace-eocenes. Strasbourg 1.

Pufahl, P.K., Grimm, K.A., 2003. Coated phosphate grains: Proxy for physical, chemical, and ecological changes in seawater. Geology 31, 801–804. https://doi.org/10.1130/G19658.1

Pufahl, P.K., Grimm, K.A., Abed, A.M., Sadaqah, R.M.Y., 2003. Upper Cretaceous (Campanian) phosphorites in Jordan: Implications for the formation of a south Tethyan phosphorite giant. Sediment. Geol. 161, 175–205. https://doi.org/10.1016/S0037-0738(03)00070-8

Pufahl, P.K., Groat, L.A., 2017. Sedimentary and igneous phosphate deposits: Formation and exploration: An invited paper. Econ. Geol. 112, 483–516. https://doi.org/10.2113/econgeo.112.3.483

Pye, K., Tsoar, H., 2009. Internal Sedimentary Structures of Aeolian Sand Deposits, in: Aeolian Sand and Sand Dunes. Springer Berlin Heidelberg, Berlin, Heidelberg, pp. 255–292. https://doi.org/10.1007/978-3-540-85910-9_7

Rauscher, R., 1985. Les dinokystes, des outils stratigraphiques pour les séries phosphatées. Application aux phosphorites du Maroc. Sci. Géologiques, Bull. mémoires 77, 69–74.

Rauscher, R., Doubinger, J., 1982. Les dinokystes du Maestrichtien phosphaté du Maroc. Sci. Géologiques. Bull. 35, 97–116. https://doi.org/10.3406/sgeol.1982.1614

Roch, E., 1939. Description géologique des montagnes à l'Est de Marrakech. Notes Mem. du Serv. Geol. du Maroc 51, 438 p.

Roth, P.H., Thierstein, H., 1972. Calcareous Nannoplankton LEG 14 Repts. DSDP, 46, Washington (U.S. Govt. Printing Office) 421-453.

Salvan, H., 1954. Les invertébrés fossiles des phosphates marocains. Notes Mémoires du Serv. Géologique du Maroc 93, 257 p.

Salvan, H.M., 1986. Géologie des gîtes minéraux marocains. Notes Mem. du Serv. Geol. du Maroc 276, 392 p.

Schettino, A., Turco, E., 2009. Breakup of Pangaea and plate kinematics of the central Atlantic and Atlas regions. Geophys. J. Int. 178, 1078–1097.

https://doi.org/10.1111/j.1365-246X.2009.04186.x

Slansky, M., 1986. Geology of sedimentary phosphates. Elsevier Science Pub. Co. Inc., New York, NY.

Soncini, M.J., 1992. Three new dinoflagellate cysts from the Moroccan Paleocene-Eocene phosphates. Rev. Palaeobot. Palynol. 70, 325–338. https://doi.org/10.1016/0034-6667(92)90070-W

Soudry, D., Nathan, Y., Ehrlich, S., 2013. Geochemical diagenetic trends during phosphorite formation - economic implications: The case of the Negev Campanian phosphorites, Southern Israel. Sedimentology 60, 800–819. https://doi.org/10.1111/j.1365-3091.2012.01361.x

Stow, D.A.V., Huc, A.Y., Bertrand, P., 2001. Depositional processes of black shales in deep water. Mar. Pet. Geol. 18, 491–498. https://doi.org/10.1016/S0264-8172(01)00012-5

Tabuce, R., Adnet, S., Cappetta, H., Noubhani, A., Quillevere, F., 2005. Aznag (bassin d'Ouarzazate, Maroc), nouvelle localité à sélaciens et mammifères de l'Eocène moyen (Lutétien) d'Afrique. Bull. la Soc. Geol. Fr. 176, 381–400. https://doi.org/10.2113/176.4.381

Teixell, A., Ayarza, P., Zeyen, H., Fernàndez, M., Arboleya, M.L., 2005. Effects of mantle upwelling in a compressional setting: The Atlas Mountains of Morocco. Terra Nov. 17, 456–461. https://doi.org/10.1111/j.1365-3121.2005.00633.x

Trappe, J., 2001. A nomenclature system for granular phosphate rocks according to

depositional texture. Sediment. Geol. 145, 135–150. https://doi.org/10.1016/S0037-0738(01)00103-8

Trappe, J., 1998. Phanerozoic Phosphorite Depositional Systems : a Dynamic Model for a Sedimentary Resource System. Springer Berlin Heidelberg.

Trappe, J., 1991. Stratigraphy, facies distribution and paleogeography of the marine Paleogene from the Western High Atlas, Morocco. Neues Jahrb. für Geol. und Paläontologie, Monatshefte 180, 279–321.

Tucholke, B.E., Sawyer, D.S., Sibuet, J.C., 2007. Breakup of the Newfoundland-Iberia rift. Geol. Soc. Spec. Publ. 282, 9–46. https://doi.org/10.1144/SP282.2

Wilmsen, M., 2003. Sequence stratigraphy and palaeoceanography of the Cenomanian Stage in northern Germany. Cretac. Res. 24, 525–568. https://doi.org/10.1016/S0195-6671(03)00069-7

Wilson, J.L., 1975. Carbonate facies in Geologic History. Springer Berlin Heidelberg.

Wright, V.P., 1994. Paleosols in shallow marine carbonate sequences. Earth-Science Rev. 35, 367–395. https://doi.org/10.1016/0012-8252(94)90002-7

Yans, J., Amaghzaz, M., Bouya, B., Cappetta, H., Iacumin, P., Kocsis, L., Mouflih, M., Selloum, O., Sen, S., Storme, J.-Y., Gheerbrant, E., 2014. First carbon isotope chemostratigraphy of the Ouled Abdoun phosphate Basin, Morocco; implications for dating and evolution of earliest African placental mammals. Gondwana Res. 25, 257–269. https://doi.org/10.1016/J.GR.2013.04.004

Zhang, Y., Pufahl, P.K., Du, Y., Chen, G., Liu, J., Chen, Q., Wang, Z., Yu, W., 2019. Economic

phosphorite from the Ediacaran Doushantuo Formation, South China, and the Neoproterozoic-Cambrian Phosphogenic Event. Sediment. Geol. 388, 1–19. https://doi.org/10.1016/J.SEDGEO.2019.05.004